

# **Electro-Optic Properties of Self-Assembled Non-Linear Optical Polymers**

**By**

**Roger G. Duncan**

This thesis has been submitted to the faculty of  
Virginia Polytechnic Institute and State University  
in partial fulfillment of the requirements for the degree of

Master of Science  
in  
Electrical Engineering

Dr. Richard Claus, Chairman

Dr. Ahmad Safaai-Jazi

Dr. Roger Stolen

April 30, 2002

Blacksburg, VA

Keywords: Self-Assembly, Electro-Optic Modulators, Non-Linear Optics, Electro-Optics,  
Interferometry, Nanotechnology

# **Electro-Optic Properties of Self-Assembled Non-Linear Optical Polymers**

Roger G. Duncan

(ABSTRACT)

Electrostatic self-assembly was used to fabricate several samples of polymers known to have non-linear optical behavior. These sample's characteristics were measured with interferometry and their electro-optic coefficients determined to be on the order of that of  $\text{LiNbO}_3$ . The self-assembled samples are shown to have an enhanced polar order compared to that of more traditional poled polymers. Furthermore, this polar order is intrinsic and thus doesn't require electric field poling and does not decay with time. The self-assembly process is therefore shown to possess great potential for the fabrication of high-speed electro-optic modulators for commercial and military applications.

## **Acknowledgments**

I would like to acknowledge many meaningful discussions with colleagues Dr. Kristie Cooper, Dr. Liangmin Zhang, Dr. You-Xiong Wang, Dr. Ken Meissner, Dr. Jeff Mecham, Mike Vercellino, Dave Wood, Carvel Holton, Jean Huie, and Fajian Zhang that have greatly contributed to both my research and the final form of this thesis.

I would like to give special thanks my advisor, Dr. Richard Claus, for all of his constant support and motivation throughout this research endeavor. I would also like to thank Dr. Roger Stolen and Dr. Ahmad Safaai-Jazi for taking the time to serve on my committee and for contributing to my professional development. It has been both an honor and a privilege.

In addition, thanks to all of the FEORC researchers and support staff for creating an environment that made the performance of this research fun.

## Table of Contents

1.	Introduction .....	1
1.1	Motivation .....	1
1.2	Scope of this Thesis .....	4
2.	The Physics of Non-Linear Optics .....	5
2.1	Introduction .....	5
2.2	Non-Linear Optical Media.....	5
2.3	Anisotropic Media .....	7
2.4	Derivation of the Electro-Optic Effect .....	10
2.5	The Electro-Optic Effect .....	12
2.6	The Molecular Origin of Optical Non-Linearity in Polymers .....	14
2.7	Polar Order .....	15
3.	Electrostatic Self-Assembly .....	17
3.1	Introduction to ESA.....	17
3.2	Processing.....	17
3.3	A Simple Model.....	18
3.4	Testing the Model.....	19
3.4	Designing for Functionality.....	22
3.6	Summary of ESA Advantages.....	23
4.	Electro-Optic Coefficient Determination .....	25
4.1	Introduction .....	25
4.2	Mach-Zehnder Interferometry .....	25
4.3	Electro-Optic Interferometry .....	27
5.	Experiment Description.....	30
5.1	Introduction .....	30
5.2	Poly S-119 .....	30
5.3	CLD-1 .....	31
5.4	Control Sample .....	32
5.5	Sample Preparation.....	33
5.6	The Measurement .....	35
6.	Results .....	38
6.1	Introduction .....	38
6.2	Separating the ‘True’ Electronic Contribution .....	38
6.3	Sample Data.....	40
6.4	Effective Voltage.....	41
6.5	Error of MZI Measurement .....	42
6.6	Results from Control Sample .....	43
6.7	Results from PS-119.....	43
6.8	Results from CLD-1 .....	45
6.9	Birefringence Contribution.....	46
7.	Discussion.....	48
7.1	Frequency Dependence.....	48
7.2	ESA vs. Spin-Coated EO Coefficients for CLD-1 .....	48
7.3	Differences in Similar ESA Fabricated Films .....	48
7.4	Suggestions for Future Work.....	49
7.5	Conclusion.....	49

## Table of Figures

Figure 1-1: Some crystal based EO modulators. ....	2
Figure 1-2: A commercially available, 40 GHz EO polymer modulator with a 0.8V switching voltage. ....	3
Figure 2-1: The projection of the electric field components along principal directions of a birefringent medium. The two components have different phase velocity so that the resultant polarization vector rotates in the direction of propagation resulting in elliptically polarized light. ....	9
Figure 2-2: Various vectors in an anisotropic medium. ....	10
Figure 2-3: Pockels Effect. ....	12
Figure 3-1: ESA schematic for buildup of multilayer assemblies by consecutive adsorption of anionic and cationic molecule-based polyelectrolytes. ....	19
Figure 3-2: ESA processing of water-soluble polymers and nanoclusters leads to multilayered thin-films with enhanced electrical, optical, thermal, and mechanical properties. ....	19
Figure 3-3: Absorbance vs. # of bilayers of PS-110/PDDA on ITO glass. ....	20
Figure 3-4: Absorbance vs. wavelength of PS-119/PDDA on ITO glass. ....	21
Figure 3-5: Material thickness vs. # of bilayers for various cation/anion self-assembled structures. ....	21
Figure 3-6: Two typical ESA films. Left-PS-119/PDDA approximately 20 nm thick. Right-PS-119/PDDA approximately 2 microns thick. ....	22
Figure 3-7: Using layer-by-layer ESA processing, thin-films may be configured to yield segmented (left), mixed (center), and graded (right) property structures. ....	23
Figure 3-8: Left-Automated dipping machine. Right-Automated vs. hand dipping. ....	24
Figure 4-1: Schematic representation of a MZI. Red-Optical radiation. Blue-Partially-silvered mirrors. Green-Mirrors. Yellow-Detectors. ....	26
Figure 4-2: MZI. L1, He-Ne Laser (632.8 nm); 1/2, half-wave plate; P, polarizer; S, sample; D, silicon photodetector; AMP, amplifier; Vdc, multimeter; HVP, high-voltage probe; LOCK-IN, lock-in amplifier, OSC, oscilloscope; WG, waveform generator; HV, high-voltage amplifier; PC, computer; W, glass translation wedge; BS's, beamsplitters; M's, mirrors; PH, pin hole; L, lens. ....	27
Figure 5-1: Left-PS-119 molecular structure. Right-PDDA molecular structure. ....	30
Figure 5-2: The molecular structure of CLD-1. ....	31
Figure 5-3: Spectral transmission characteristics of NOA63. ....	33
Figure 5-4: Preparing the samples for measurement. ....	34
Figure 5-5: The MZI. ....	35
Figure 5-6: The MZI in action. ....	35
Figure 6-1: An example of the data collected. ....	40
Figure 6-2: Model of the sample 'sandwich'. ....	41
Figure 6-3: Electro-optic coefficients of Control-1. ....	43
Figure 6-4: Summary of PS-119 data. EO coefficient values are taken at 1 kHz. ....	43
Figure 6-5: r33 of PS-119 samples. ....	44
Figure 6-6: r13 of PS-119 samples. ....	44
Figure 6-7: r33 of CLD-1. ....	45
Figure 6-8: r13 of CLD-1. ....	46
Figure 6-9: Responsivity of ESA fabricated CLD-1. ....	47

Figure 6-10: Responsivity of ESA fabricated CLD-1. Birefringence contribution is obvious at very low frequencies but quickly dies out. ....47

# 1. Introduction

---

## **1.1 Motivation**

As the need for bandwidth in telecommunications applications grows, techniques and devices that allow more efficient use of the extraordinary bandwidth potential of optical fibers become more and more important. The highest bandwidth standard for a fiber channel in the United States is only 2.5 Gbit/s (OC-48), while Nortel in Canada uses a higher standard at 10 Gbit/s (OC-192). These bit rates represent only a fraction of available bandwidth of optical fibers. Perhaps the biggest bottleneck to more efficient usage is the speed of electrical to optical conversions. Current communications systems primarily make use of internal modulation, which is a direct modulation of the optical source by changing the supplied current. However, this method is limited to relatively low speeds because of chirp. External modulation is a potentially superior approach that separates the functions of the transmitter of a communication system.

Of the many types of external modulators, perhaps only two are currently commercially feasible approaches. Electro-adsorption and electro-optic (EO) modulators both use voltage regulated phenomena to encode the optical carriers. However, electro-adsorption modulators also suffer from large chirp and have wavelength selectivity issues which make them difficult to mass produce. Electro-Optic modulators are a more commercially viable technology.

Since their discovery, significant advances in electro-optic modulators have attracted great interest because of their potential applications in ultra-high speed information transmission and processing. Current commercial EO modulators take advantage of solid-state crystals (See Fig. 1-1) such as  $\text{LiNbO}_3$  and have switching voltages typically in the range of 3-5 V so that broadband amplifiers are required to drive the modulators, limiting bandwidth considerably. Even so, 20 GHz  $\text{LiNbO}_3$  modulators have been fabricated and sold commercially.



**Figure 1-1: Some crystal based EO modulators.**

More to the point, crystal based EO modulators have physically limited bandwidths at approximately 40 GHz. This is a material limitation and cannot be bypassed. Therefore, at best,  $\text{LiNbO}_3$  represents a stopgap solution.

In comparison to inorganic crystal-based modulators, organic polymer devices offer potential advantages of large bandwidths and low switching voltages. This is because organic polymers have low dielectric constants<sup>1</sup>, which, given traveling wave modulator geometries, permit the optical and microwaves to propagate with nearly equal phase velocities. Moreover, organic polymers offer the promise of exceptionally high EO coefficients, which is a very important factor in reducing the switching voltage<sup>2,3</sup>.

---

<sup>1</sup> S. J. Lalama, and A. F. Garito, *Phys. Rev. A* 20, 1179 (1979).

<sup>2</sup> Y. G. Zhao, A. Wu, H. L. Lu, S. Chang, W. K. Lu, S. T. Ho, M. E. van der Boom, and T. J. Marks, *Appl. Phys. Lett.* 79 (5), 589 (2001).

<sup>3</sup> C. Zhang, M. C. Oh, H. Zhang, W. H. Steier, and L. R. Dalton, *Chem. Mater.* 13, 3043 (2001).

Multiple high speed, wide-bandwidth EO polymer modulators with simple microstrip line electrodes have been demonstrated over the years<sup>4</sup>, but their switching voltages have been on the order of 3.5-5V. However, recent advances in the theoretical modeling of chromophore interactions and material synthesis have resulted in many new non-linear optical chromophores, which have, in turn, resulted in major advances in EO polymer modulator fabrication and have yielded a device with a 0.8V switching voltage<sup>5,6</sup> and a 40 GHz bandwidth. This device is currently commercially available (See Fig. 1-2) from Pacific Wave Industries Inc., which is a company founded by members of the group responsible for the invention. EO polymer modulators having bandwidths as high as 110 GHz have been demonstrated<sup>7</sup>.



**Figure 1-2: A commercially available, 40 GHz EO polymer modulator with a 0.8V switching voltage.**

<sup>4</sup> D. Chen, H. R. Fetterman, A. Chen, W. H. Steier, L. R. Dalton, W. Wang, and Y. Shi, Appl. Phys. Lett. 70, 3335 (1997).

<sup>5</sup> Y. Shi, W. Lin, D. J. Olson, J. H. Bechtel, H. Zhang, W. H. Steier, C. Zhang, and L. R. Dalton, Appl. Phys. Lett. 77, 1 (2000).

<sup>6</sup> Y. Shi, C. Zhang, H. Zhang, J. H. Bechtel, L. R. Dalton, B. H. Robinson, and W. H. Steier, Science 288, 119 (2000).

<sup>7</sup> D. Chen, H. R. Fetterman, A. Chen, W. H. Steier, L. R. Dalton, W. Wang, and Y. Shi, Appl. Phys. Lett. 70, 3335 (1997).

## ***1.2 Scope of this Thesis***

This thesis investigates the viability of utilizing a self-assembled processing method for the reliable manufacture of EO polymer modulators. It furthers the work done in this area by many researchers at VPI's Fiber and Electro-Optic Research Center (FEORC), as well as groups elsewhere. Along these lines, this thesis investigates the EO properties of some self-assembled polymers, and where appropriate, makes relevant comparisons to poled polymers. It is this author's intention to show that self-assembled polymer films do indeed have an intrinsic polar order and are superior in many ways to more traditional poled polymers, and may indeed offer a commercially viable alternative.

## 2. The Physics of Non-Linear Optics

---

### 2.1 Introduction

This chapter summarizes the physics of non-linear optics. Using Maxwell's equations, a qualitative description of the interaction of light with a bulk media, as it relates to non-linear optical phenomena, is derived. Some mathematical detail is present where deemed necessary for illustration, but generally a descriptive approach is favored. A rigorous and complete mathematical treatment of electromagnetic field theory, linear, and non-linear optics, is outside the scope of this thesis.

### 2.2 Non-Linear Optical Media

A molecular medium, such as an organic crystalline or polymeric solid, is generally non-conducting and non-magnetic and the electrons are regarded as being tightly bound to the nuclei. For such media, the interaction with light can generally be regarded within the framework of a dielectric subjected to an electric field. This approach is referred to as the dipole approximation because the charge distribution induced in the molecule by the field is readily approximated by that of an induced dipole. The applied field polarizes the molecules in the medium, displacing them from their equilibrium positions and induces a dipole moment,  $\mu_{ind}$ , given by

$$\mu_{ind} = -er, \quad (1)$$

where  $e$  is the electronic charge and  $r$  is the field induced displacement. The bulk polarization  $P$  resulting from this induced dipole is given by

$$P = -Ner, \quad (2)$$

where  $N$  is the electron density in the medium.

The electric field inside the material is lowered by the polarization that opposes the externally applied field. The reduction in field intensity in the volume element containing the molecule of interest is by the factor  $1 + \epsilon$ , where  $\epsilon$  is the dielectric constant of the medium. If the field strength is relatively low, the polarization of the medium is linear in the applied field. The linear polarization is expressed in terms of a susceptibility  $\chi^{(1)}$  as

$$P = \chi^{(1)} \cdot E, \quad (3)$$

where the susceptibility is related to the dielectric constant by<sup>8</sup>

$$\epsilon = 1 + 4\pi \cdot \chi^{(1)}. \quad (4)$$

When a medium is subject to an intense electric field such as that due to an intense laser pulse, the polarization response of the material is not adequately described by the previous equation. Assuming that the polarization of the medium is still weak compared to the binding forces between the electrons and the nuclei, the polarization can be expressed in a power series of the field strength  $E$ <sup>9</sup>

$$P = \chi^{(1)} \cdot E + \chi^{(2)} : EE + \chi^{(3)} : EEE + \dots, \quad (5)$$

which I shall refer to as the polarization expansion equation<sup>10,11</sup>.

Note that for sake of brevity, tensor notation is used, where

$$\chi^{(2)} : EE = \sum_{J,K} \chi_{JK}^2 E_J E_K. \quad (6)$$

---

<sup>8</sup> E. Riande, E. Saiz, *Dipole Moments and Birefringence of Polymers*, edited by J. E. Marks, Prentice Hall, Englewood Cliffs, New Jersey 1992.

<sup>9</sup> G. R. Fowles, *Introduction to Modern Optics*, Dover Publications, Inc., New York 1989.

<sup>10</sup> *Polymers for Second-Order Nonlinear Optics*, edited by G. A. Lindsay and K. D. Singer, American Chemical Society, Washington, D. C. 1995.

<sup>11</sup> K. D. Singer, M. G. Kuzyk, and J. E. Sohn, *J. Opt. Soc. Am. B* 4 (6), 968 (1987).

In the above polarization equation, the term that is quadratic in the field strength  $E$  describes the first non-linear effect. The coefficient,  $\chi^{(2)}$ , relating the polarization to the square of the field strength  $E$ , is called the second-order nonlinear susceptibility of the medium and is a third-rank tensor.

The manifestation of non-linear optical phenomena can be clearly seen by substituting a sinusoidal field equation into the polarization equation above and applying appropriate trigonometric identities. This yields

$$P = \chi^{(1)} E_0 \cos(\omega t - kz) + \frac{1}{2} \chi^{(2)} E_0^2 [1 + \cos(2\omega t - 2kz)] + \chi^{(3)} E_0^3 \left[ \frac{3}{4} \cos(\omega t - kz) + \frac{1}{4} \cos(3\omega t - 3kz) \right]. \quad (7)$$

This equation clearly shows the presence of new frequency components due to the non-linear polarization. The second-order term gives a frequency independent contribution as well as one at  $2\omega$ . The former suggests that a dc polarization should appear in a second-order non-linear material when it is appropriately irradiated. This phenomenon is referred to as optical rectification. The latter term corresponds to Second-Harmonic Generation (SHG). The third term indicates a frequency response at the frequency of the optical field  $\omega$  as well as a response at  $3\omega$ . The even and odd-order terms in the expansion therefore lead to fundamentally different types of non-linear responses. The contributions from the different terms to the non-linear polarization are predicated from different symmetry properties of the media. A contribution from  $\chi^{(2)}$  can come only from non-centrosymmetric media, whereas  $\chi^{(3)}$  contributions can come from any medium, regardless of symmetry<sup>12</sup>.

### **2.3 Anisotropic Media**

In general, materials likely to be of interest in non-linear optics are not likely to be isotropic. Organic crystals, for instance, are composed of molecules having definite orientations within the unit cell and the molecules themselves often have highly

---

<sup>12</sup> P. N. Prasad, D. J. Williams, *Introduction to Nonlinear Optical Effects in Molecules and Polymers*, John Wiley & Sons, Inc. 1991.

anisotropic electronic structures. Therefore, polarization response in directions other than that of the applied electric fields might be expected. Similarly, polymer chains in a solid are often oriented other than randomly and the exact nature of their orientational distribution will determine their response. For this reason, the susceptibilities are tensor quantities relating the polarization response in one direction to field components in three directions. For the purposes of this thesis, the anisotropic phenomenon of interest is the dielectric constant  $\epsilon_{ij}$ , which relates the electric field and the dielectric displacement and is a second-rank tensor.

The most interesting consequence of this dielectric anisotropy is the phenomenon of birefringence. Visualizing a uniaxial crystal with  $n_x = n_y \neq n_z$ , where  $n$  is the materials index of refraction and is given as

$$n \approx \sqrt{\epsilon} , \quad (8)$$

and with a lightwave propagating from left to right along the x-axis with its electric field polarized in the z-direction (See Fig. 2-1). The propagation constant  $k_z$  will be determined by  $n_z$  from

$$k_z = \frac{\omega}{c} n_z . \quad (9)$$

Another wave, propagating along the x-direction but with y-polarization, would have a different propagation constant  $k_y$ . The waves would accumulate a phase difference traveling through the crystal. If the waves were a projection of a plane wave incident from the x-direction with a  $45^\circ$  inclination from the z-axis, then the cumulative phase lag would cause the resultant electric field vector to rotate as it propagated, resulting in elliptically polarized light.

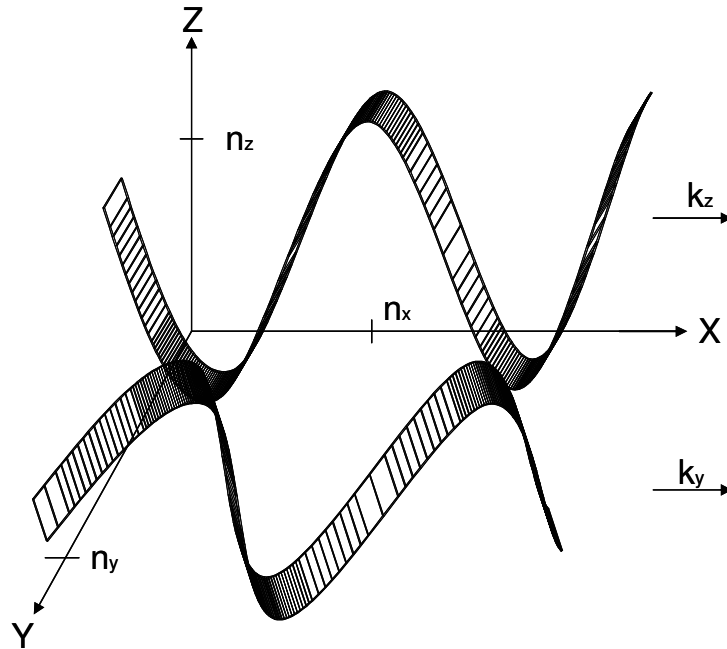


**Figure 2-1: The projection of the electric field components along principal directions of a birefringent medium. The two components have different phase velocity so that the resultant polarization vector rotates in the direction of propagation resulting in elliptically polarized light.**

A further consequence of birefringence is that for light incident in any direction, other than along a principal axis, the flow of energy isn't normal to the wavefront. In a vacuum or isotropic medium the wavefront perpendicular to the propagation direction is always parallel to energy flow. In anisotropic media, this is not the case except for the condition stated above.

This point can be illustrated in a conceptual way. The electric  $E$  and magnetic  $H$  vectors of the incident wave are always mutually orthogonal. The electric vector produces a dielectric displacement  $D$  which is in general not parallel to  $E$ . The magnetic vector  $H$  produces a magnetic induction  $B$ , but which is for all practical purposes parallel to  $H$  because of the weakness of the interaction of  $H$  with a non-magnetic medium. The propagation of the wavefront in the crystal is perpendicular to  $D$  and  $H$  but the flow of power  $S$ , also known as the Poynting vector, as required by Maxwell's equations, is

proportional to  $E \times H$ . In other words, the propagation of the polarization wave and the flow of optical power are not parallel (See Fig. 2-2)<sup>13</sup>.

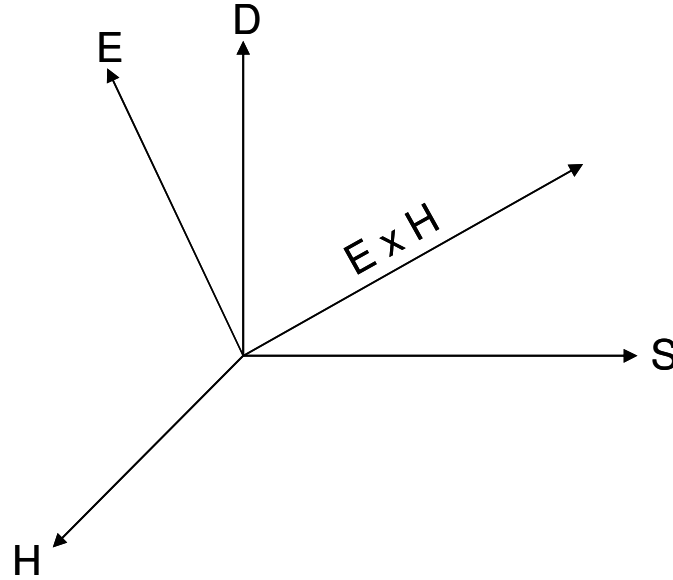


Figure 2-2: Various vectors in an anisotropic medium.

## 2.4 Derivation of the Electro-Optic Effect

Assume a medium is subjected to a DC (or low-frequency AC) electric field, which is designated as  $E(0)$ , and an optical field  $E(\omega)$ . The total field the medium is subject to is therefore

$$E = E(0) + E(\omega) = E(0) + E_0 \cos(\omega t - kz). \quad (10)$$

Substituting this field into the polarization expansion equation and applying the appropriate trigonometric identities, and collecting terms that describe oscillation at  $\omega$ , gives

$$P(\omega) = \chi^{(1)} E_0 \cos(\omega t - kz) + 2\chi^{(2)} E(0) E_0 \cos(\omega t - kz) + 3\chi^{(3)} E^2(0) E_0 \cos(\omega t - kz) + \frac{3}{4} \chi^{(3)} E_0^3 \cos(\omega t - kz). \quad (11)$$

<sup>13</sup> *Nonlinear Optical Properties of Organic and Polymeric Materials*, edited by D. J. Williams, American Chemical Society, Washington, D. C. 1983.

Which can also be written as

$$P(\omega) = \chi_{\text{eff}} E(0) \cos(\omega t - kz). \quad (12)$$

Relating this to the medium's index of refraction yields

$$n^2 = 1 + 4\pi\chi_{\text{eff}}. \quad (13)$$

Designating the linear refractive index as  $n_0$ , and performing appropriate substitutions, leads to the relationship

$$n = n_0 + \frac{4\pi\chi^{(2)}}{n_0} E(0) + \frac{6\pi\chi^{(3)}}{n_0} E(0)^2 + \frac{3\pi}{2n_0} \chi^{(3)} E_0^2. \quad (14)$$

The definition of the light intensity in cgs units is

$$E_0^2 = \frac{8\pi}{cn} I(\omega), \quad (15)$$

which when substituted into the previous equation yields

$$n = n_0 + \frac{4\pi\chi^{(2)}}{n_0} E(0) + \frac{6\pi\chi^{(3)}}{n_0} E(0)^2 + \frac{12\pi}{cn_0^2} \chi^{(3)} I. \quad (16)$$

The value of the non-linear index of refraction at frequency  $\omega$  can therefore be written as

$$n(\omega) = n_0(\omega) + n_1 E(0) + n_2(0) E(0)^2 + n_x(\omega) I(\omega) \quad (17)$$

where the terms  $n_1$ ,  $n_2(0)$ , and  $n_x(\omega)$  are defined as

$$n_1 = \frac{4\pi\chi^{(2)}}{n_0}, \quad (18)$$

$$n_2(0) = \frac{6\pi\chi^{(3)}}{n_0}, \quad (19)$$

$$n_2(\omega) = \frac{12\pi\chi^{(3)}}{cn_0^2}, \quad (20)$$

respectively, and correspond to the linear electro-optic (EO) effect, also known as Pockels effect, the quadratic electro-optic effect, and the Kerr effect. This thesis primarily concerns itself with the linear electro-optic effect.

## 2.5 The Electro-Optic Effect

The linear electro-optic effect is the change in the index of refraction that occurs when an external electric field is applied to a material with a non-centrosymmetric structure.

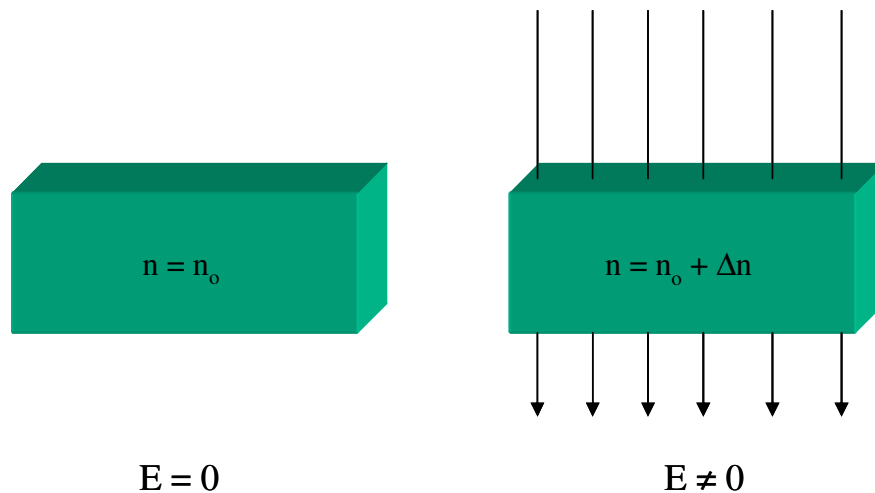


**Figure 2-3: Pockels Effect.**

This index change is proportional to the applied electric field and is given by

$$\Delta n = -\frac{n^3}{2} rE \quad (21)$$

where  $\Delta n$  is the change of the material's optical index of refraction, and  $r$  is called the electro-optic coefficient.

For an anisotropic dielectric media, the electro-optic coefficient comes from the electric field induced distortion of the index ellipsoid<sup>14</sup>:

$$\frac{x^2}{n_1^2} + \frac{y^2}{n_2^2} + \frac{z^2}{n_3^2} + 2\frac{yz}{n_4^2} + 2\frac{zx}{n_5^2} + 2\frac{xy}{n_6^2} = 1. \quad (22)$$

When  $x, y, z$  were chosen as the mediums principal axes, without the external field,

$$\frac{1}{n_1^2} = \frac{1}{n_x^2}, \quad (23)$$

$$\frac{1}{n_2^2} = \frac{1}{n_y^2}, \quad (24)$$

$$\frac{1}{n_3^2} = \frac{1}{n_z^2}, \quad (25)$$

$$\frac{1}{n_4^2} = \frac{1}{n_5^2} = \frac{1}{n_6^2} = 0, \quad (26)$$

where  $n_x, n_y,$  and  $n_z$  are the respective half lengths of the index ellipsoid along the  $x, y,$  and  $z$  directions.

---

<sup>14</sup> M. A. Karim, *Electro-Optical Devices and Systems*, edited by J. Plant, PWS-Kent Publishing Company, Boston, Massachusetts, 1990.

When an external electric field is applied to the medium, the index ellipsoid is slightly distorted

$$\Delta\left(\frac{1}{n^2}\right) = r \cdot E \quad (27)$$

where the electro-optic coefficient,  $r$ , is a second rank tensor<sup>15</sup>

$$\Delta \begin{bmatrix} \frac{1}{n_1^2} \\ \frac{1}{n_2^2} \\ \frac{1}{n_3^2} \\ \frac{1}{n_4^2} \\ \frac{1}{n_5^2} \\ \frac{1}{n_6^2} \end{bmatrix} = \begin{bmatrix} r_{11} & r_{12} & r_{13} \\ r_{21} & r_{22} & r_{23} \\ r_{31} & r_{32} & r_{33} \\ r_{41} & r_{42} & r_{43} \\ r_{51} & r_{52} & r_{53} \\ r_{61} & r_{62} & r_{63} \end{bmatrix} \begin{bmatrix} E_1 \\ E_2 \\ E_3 \end{bmatrix}. \quad (28)$$

From this it is seen that the electro-optic tensor has 18 terms, however, due to various material symmetries, most of these values will be equal to zero.

## **2.6 The Molecular Origin of Optical Non-Linearity in Polymers**

Typically, Non-Linear Optical Polymer (NLOP) films are glassy polymers containing asymmetric chromophores. It is these chromophores, which are seen as net dipoles, which are the origin of optical non-linearity in polymers. When non-centrosymmetric molecules form bulk material, the molecular orientation, either random or with a certain symmetry, may introduce an orientational centrosymmetry. This orientational

---

<sup>15</sup> D. Chen, "High Speed Polymer Modulators", Ph.D. dissertation, Electrical Engineering Dept., University of California, Los Angeles, 1997.

centrosymmetry will tend to cancel the individual molecular contribution to  $\chi^{(2)}$ , resulting in a zero bulk non-linearity. Therefore it is important to ensure that all the non-centrosymmetric molecules are properly aligned.

## **2.7 Polar Order**

The most widely used technique to remove centrosymmetry (i.e.-to impart polar order) in a polymer film is electric field poling<sup>16</sup>. In this technique films are prepared for poling by spin-coating a liquid solution of the polymer onto a solid substrate. The poling process is the application of an electric field applied across the film, with the film heated to near its glass transition temperature ( $T_g$ ), as it sits on a grounded conductor. Typically these electric fields are hundreds of volts per micron of film. The electric field is thus applied for approximately an hour, and then the film is cooled, while the electric field remains applied. Generally, the non-linear optic coefficients increase linearly with poling field until a saturation condition exists. The degree of alignment is proportional to

$$\mu E / kT , \quad (29)$$

where  $\mu$  is the ground state dipole moment of the chromophore,  $E$  is the applied electric field,  $k$  is Boltzmann's constant, and  $T$  is the poling temperature.

There are several problems with electric field poling. The polymer must be heated to high temperatures where thermal disordering of the chromophores works against the torque of the electric field and may damage the surface of the film, causing defects. Also, after the electric field is removed, the torque is gone and thermal vibration will tend to destroy the molecular alignment again. Techniques exist, such as crosslinking of molecules, that can slow this process, and indeed may maintain some reasonable polar order for some years, but it cannot be completely halted. What is needed is a technique to 'freeze' the molecular orientation.

---

<sup>16</sup> *Polymers for Second-Order Nonlinear Optics*, edited by G. A. Lindsay and K. D. Singer, American Chemical Society, Washington, D. C. 1995.

This is where self-assembled films come into play. Self-Assembled films, unlike poled polymers, tend to have an intrinsic molecular dipolar alignment that does not decay with time, removing the need for electric field poling and removing the primary obstacle to commercially viable polymer-based electro-optic modulators.

## 3. Electrostatic Self-Assembly

---

### 3.1 Introduction to ESA

The basic principle behind Electrostatic Self-Assembly (ESA) is the alternate adsorption of oppositely charged polyions on a charged substrate<sup>17</sup>. A wide variety of molecules, including nonlinear optical chromophores<sup>18</sup>, conducting polymers<sup>19</sup>, biological macromolecules, magnetic materials, metallic or metallic oxide nanoparticles, and dielectrics may be incorporated into the film to achieve specific functionality. Appropriately choosing molecules and adjusting the deposition parameters allows precision control over the composition and structure of each layer. This makes ESA practical for a wide variety of applications including, but not limited to, novel films and structures for photonic applications. This section therefore reviews the basic model of this process and explains the formation of thin-films and structures having required functional properties.

### 3.2 Processing

First, the substrates require pre-treatment before applying the multilayer films. The common substrates such as quartz, glass, and single crystal silicon are first cleansed with a 30:70 mixture of hydrogen peroxide ( $H_2O_2$ ) and concentrated sulfuric acid ( $H_2SO_4$ ), called 'piranha solution', at room temperature for one hour<sup>20</sup>. The substrate is then cleaned using ultra-pure water and dried in an oven at 50°C for several hours. This process 'functionalizes' the substrate, giving it a negative charge. For Indium-Tin-Oxide (ITO) coated glass substrates, a slightly different process is used to prevent the stripping off of the ITO coating. For these, the cleaning is done twice in ethanol, using an

---

<sup>17</sup> Y. J. Liu, A. Wang, and R. O. Claus, *Appl. Phys. Lett.* 71 (16), 2265 (1997).

<sup>18</sup> L. M. Zhang, F. Zhang, K. Cooper, Y. X. Wang, Y. J. Liu, and R. O. Claus, *Opt. Comm.* 186, 135 (2000).

<sup>19</sup> Y. J. Liu, Y. X. Wang, and R. O. Claus, *Chem. Phys. Lett.* 298, 315 (1998).

<sup>20</sup> A. Chandran, "Self-Assembled Multilayered Dielectric Spectral Filters", M.S. thesis, Electrical Engineering Dept., Virginia Polytechnic Institute & State University, Blacksburg, Virginia, September 2001.

ultrasonic agitation system. It is then immersed in a 1:1 mixture of ethanol and sulfuric acid at room temperature for one hour and then rinsed in ultra-pure water.

A monolayer of polyelectrolyte is assembled on the oppositely charged substrate through ionic bonding, by dipping the substrate in the ionic solution. After rinsing this now coated substrate in ultra-pure water to remove the loosely adsorbed molecules, the substrate is then immersed in an oppositely charged polyelectrolyte solution to adsorb the next molecular monolayer. The resulting coated substrate is again rinsed in ultra-pure water. Thus, one bilayer (cation/anion) is synthesized. Repeating this process, we get multilayer structures.

### ***3.3 A Simple Model***

First, the formation of alternating monolayers of simple polymer polyelectrolytes alone is shown in Figure 3-1. On the left, the substrate surface has been thoroughly cleaned and functionalized, so the outermost surface effectively has a net negative charge. It is assumed that this net surface-charged substrate is dipped into a solution containing water soluble cation polymer molecules that have net positively charged functional groups fixed to their polymer backbone.

Because the polymer chain is flexible, it is free to orient its geometry with respect to the substrate prior to bond formation, so a relatively low energy molecular configuration is achieved locally. Some of the positively charged functional groups along the polymer chain experience attractive ionic forces toward the negative substrate, and the polymer chain is bent as shown in response to those combined forces. The net negative charge on the substrate is thus masked from other positive groups along the polymer chain. Those groups thus feel a force due to the fixed positive functional groups bonded to the substrate surface, so move away from that surface to form a net positive charge distribution on the outermost surface of the coated substrate. Since the total polymer layer is neutral, negative charges with relatively loose binding to the polymer network pair up with positive ions. Subsequent polyanion and polycation monolayers are added, to produce the multilayer structure as shown.

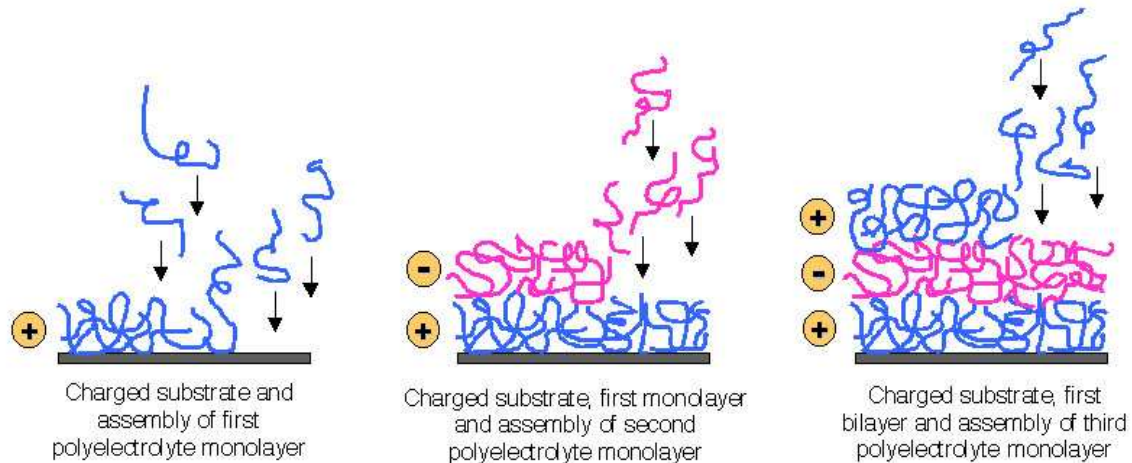


**Figure 3-1: ESA schematic for buildup of multilayer assemblies by consecutive adsorption of anionic and cationic molecule-based polyelectrolytes.**

Figure 3-2 shows a similar method of ESA processing where appropriately charged quantum dots are substituted for one of the polymer layers. FEORC has used this polymer/particle model to design, synthesize and demonstrate materials that display a broader range of electrical, optical, mechanical and thermal properties than obtainable using polymer molecules alone.

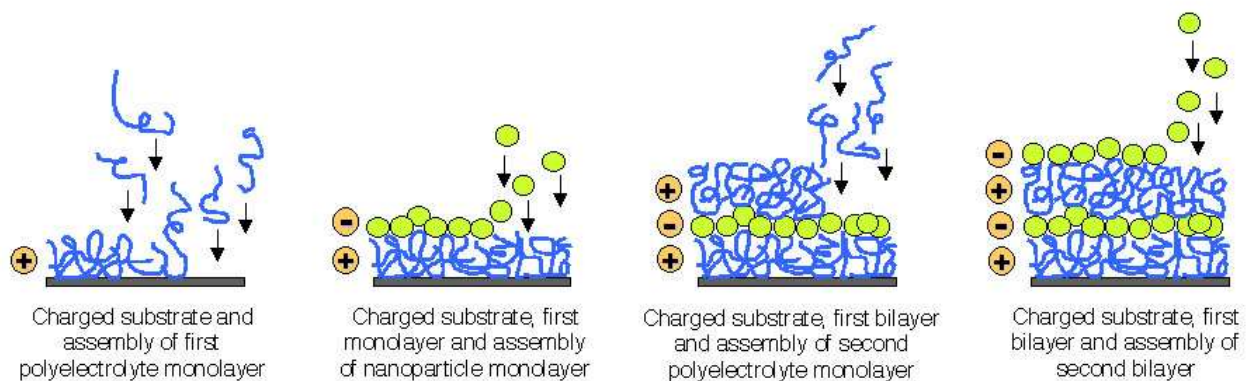


**Figure 3-2: ESA processing of water-soluble polymers and nanoclusters leads to multilayered thin-films with enhanced electrical, optical, thermal, and mechanical properties.**

### **3.4 Testing the Model**

If this simple model of the ESA process is correct, then one may hypothesize that for a relatively small number of bilayers (<1000), certain properties such as material

absorbance and material thickness increase linearly with the number of bilayers<sup>21,22,23</sup>. This is tested easily enough with spectrophotometry. Figures 3-3 and 3-4 demonstrate material absorbance of a self-assembled PS-119/PDDA sample on ITO coated glass. An absorbance peak for the material can be seen at approximately 475 nm, whereas the ITO coated glass substrate absorbs heavily in the UV. Note that the absorbance does indeed increase linearly with the number of bilayers, as expected. Figure 3-5 shows how material thickness of various cation/anion self-assembled structures increases with number of bilayers, as measured with ellipsometry. This too indicates linear growth. Figure 3-6 shows two typical ESA samples. Both pictured are PS-119/PDDA, but the film on the left is approximately 50 nm, while the film on the right is approximately 2  $\mu\text{m}$ . Note the obvious differences in transparency.

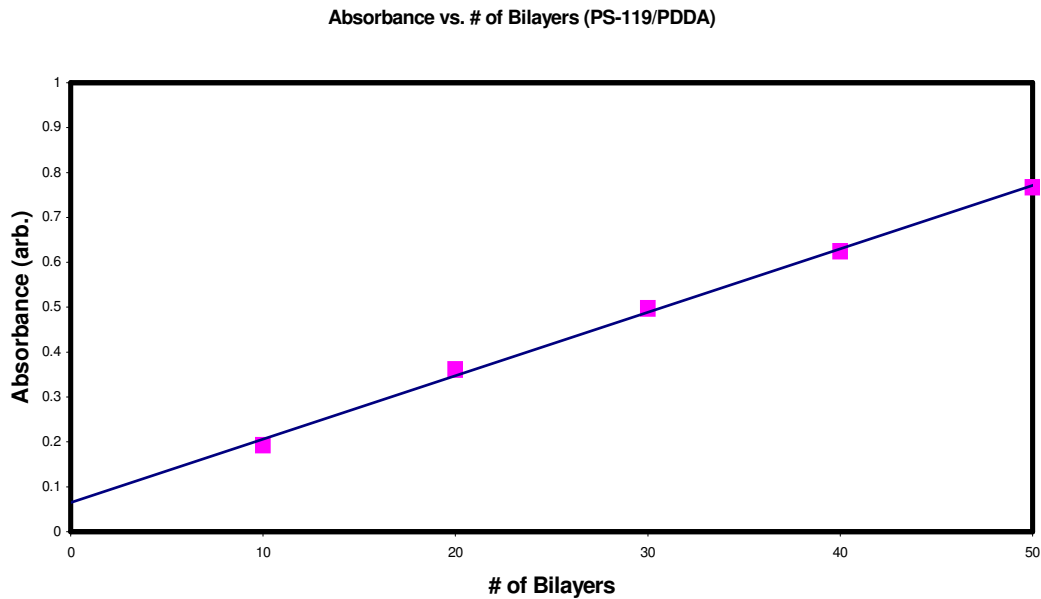


**Figure 3-3: Absorbance vs. # of bilayers of PS-110/PDDA on ITO glass.**

---

<sup>21</sup> K. Cooper, "Electrostatic self-assembly of linear and nonlinear optical thin films", Ph.D. dissertation, Electrical Engineering Department, Virginia Polytechnic Institute and State University, Blacksburg, Virginia, May 1996.

<sup>22</sup> Y. J. Liu, A. Rosidian, K. Lenahan, Y. X. Wang, T. Zeng, and R. O. Claus, *Smart Mater. Struct.* 8, 100 (1999).

<sup>23</sup> J. R. Heflin, C. Figura, D. Marciu, Y. J. Liu, and R. O. Claus, *Appl. Phys. Lett.* 74 (4), 495 (1999).

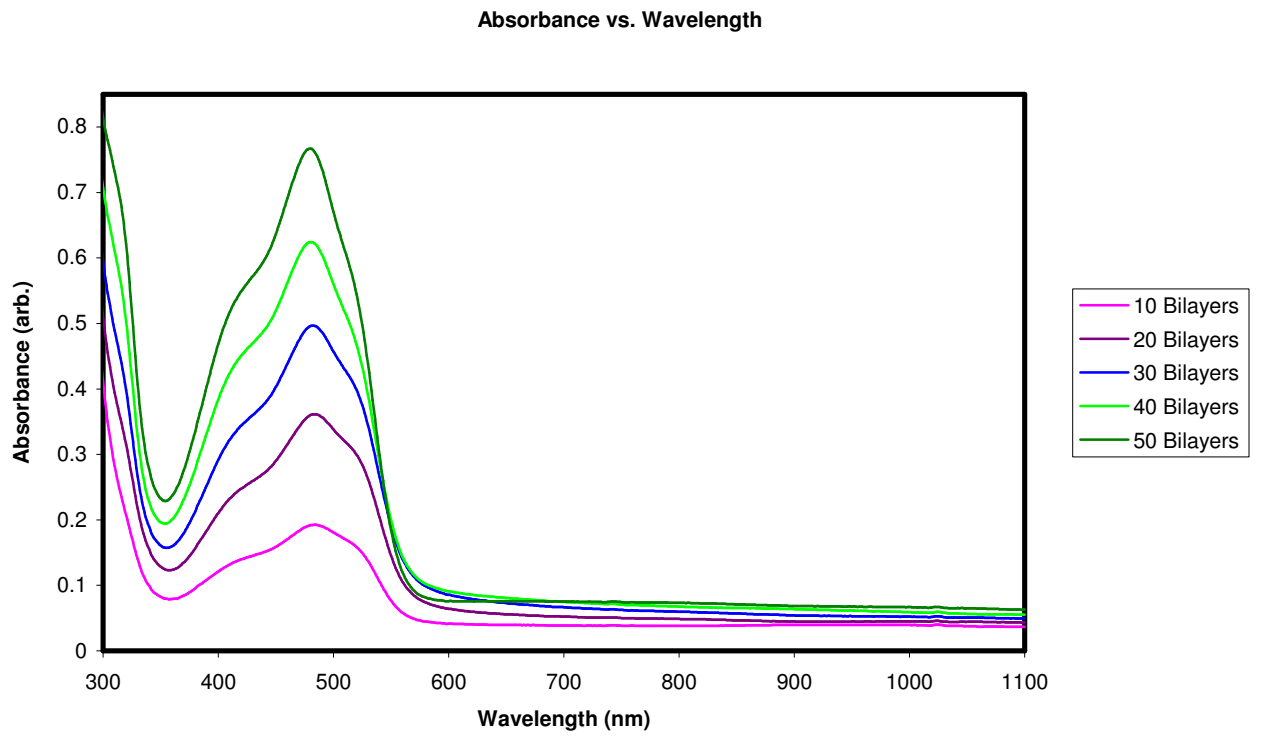


Figure 3-4: Absorbance vs. wavelength of PS-119/PDDA on ITO glass.

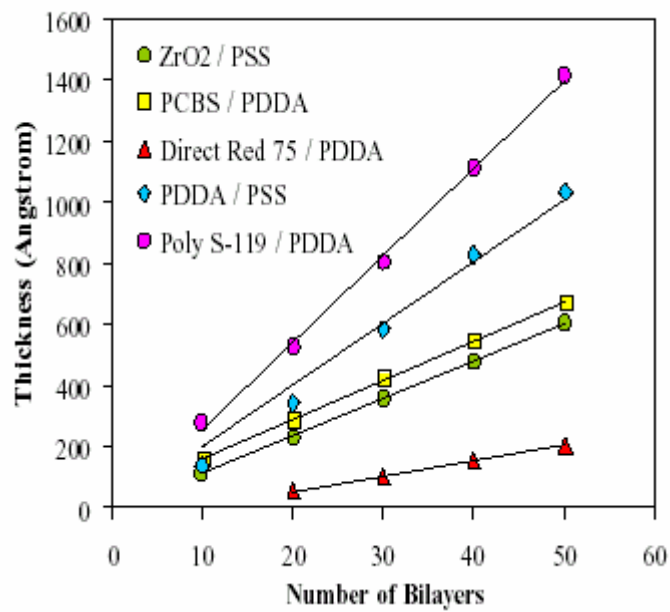
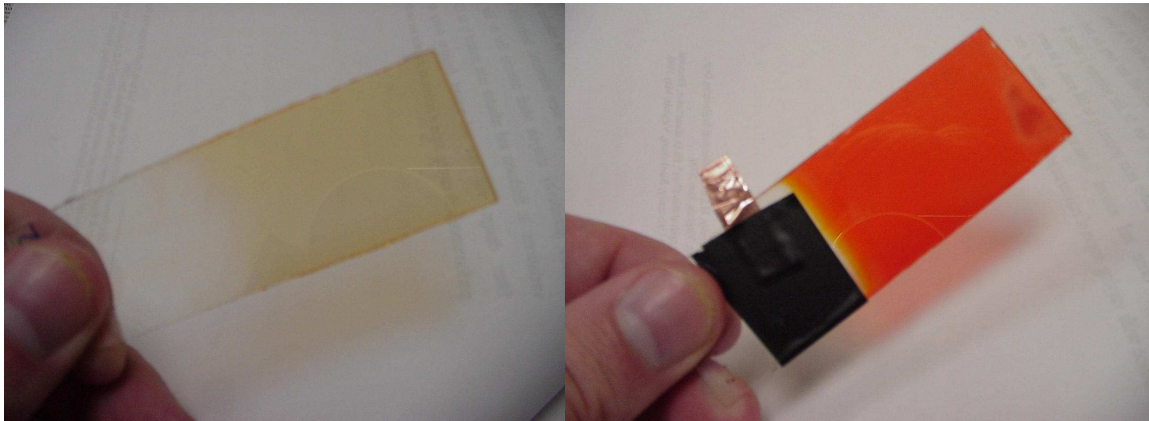


Figure 3-5: Material thickness vs. # of bilayers for various cation/anion self-assembled structures.



**Figure 3-6: Two typical ESA films. Left-PS-119/PDDA approximately 20 nm thick. Right-PS-119/PDDA approximately 2 microns thick.**

### ***3.4 Designing for Functionality***

The next part of the ESA processing model that is important is the ability to vary the dielectric constant or other properties through a multilayer structure by the ESA process itself, as well as laterally in the plane of the substrate by post-deposition patterning. This allows the formation of novel structures.

As an example of the versatility of the ESA fabrication process, Figure 3-7 shows three different layer-by-layer “basis function” models that have been considered as part of prior research that may be useful in the design and synthesis of numerous device structures. The multi-segmented geometry shown at the left of Figure 3-7 may be used to implement a simple waveguide structure consisting of a central core region and surrounded on both top and bottom by ESA-formed cladding layers.

The stacks shown here may be of potentially two molecular forms. The first alternative, shown in the center of Figure 3-7, is that different materials AB and AC are combined through the thickness of the material. As shown below based on FEORC experimental results, by controlling the relative percentages of AB and AC materials in the total

thickness, the resulting properties, for example the effective complex dielectric constant, may be controlled<sup>24</sup>.

The second alternative, not easily implemented using poled polymer and spin coating methods, is shown at the right in Figure 3-7. Here, a graded property coating is diagrammed, suggesting that by gradually changing the relative percent contributions of two or more constituents versus distance through the cladding, graded properties may be realized. This particular ability would be extremely useful in fabricating EO modulators because of the possibility of graded index waveguide claddings.

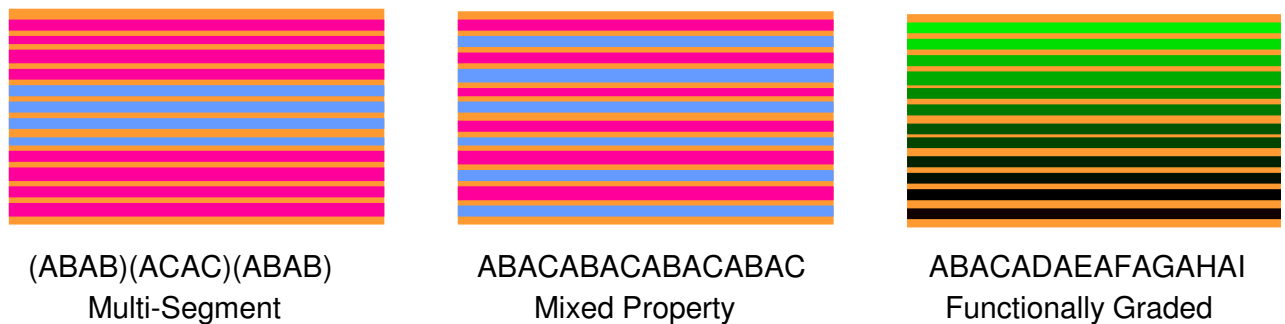


Figure 3-7: Using layer-by-layer ESA processing, thin-films may be configured to yield segmented (left), mixed (center), and graded (right) property structures.

### 3.6 Summary of ESA Advantages

In comparison with conventional manufacturing methods, ESA processing thus has the following known advantages for the fabrication of EO devices:

- **Flexibility** Devices of required electrical, optical, mechanical, and thermal properties may be designed to give the desired net macroscopic effects.
- **Ease of Fabrication** ESA films may be fabricated in room temperatures and pressures with the simple dip, rinse, dip procedure lending itself well to automation.

<sup>24</sup> Y. J. Liu, Y. X. Wang, and R. O. Claus, Chem. Phys. Lett. 298 (4-6), 315 (1998).

- **Precision Control** Layer and segment thickness through the film structure may be precisely controlled.
- **Compatibility** ESA is fully compatible with conventional low-cost lithographic techniques.
- **Environment Friendly** ESA is an environmentally friendly process, involving no volatile organic compounds and consuming negligible electrical power.

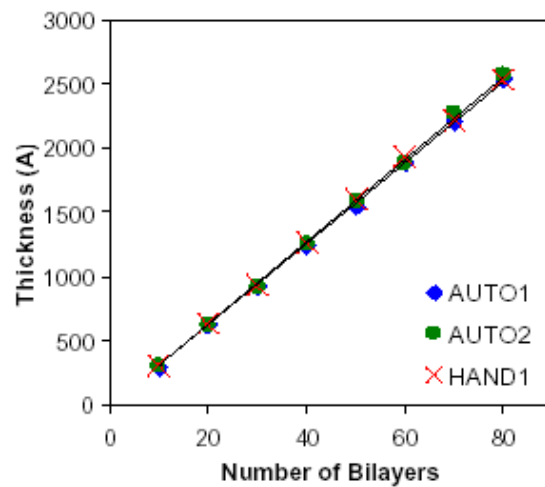


Figure 3-8: Left-Automated dipping machine. Right-Automated vs. hand dipping<sup>25</sup>.

<sup>25</sup> K. Cooper, “Electrostatic self-assembly of linear and nonlinear optical thin films”, Ph.D. dissertation, Electrical Engineering Department, Virginia Polytechnic Institute and State University, Blacksburg, Virginia, May 1996.

## 4. Electro-Optic Coefficient Determination

---

### 4.1 Introduction

As previously stated, the primary scope of this thesis is the characterization of electro-optic polymers fabricated with the self-assembly process. To this end, it is recognized that there are a number of techniques that are used to measure the electro-optic properties of polymer films<sup>26,27,28,29</sup>. One popular method is the reflection technique, in which an amplitude modulation is detected that results from beating the modulation of a wave polarized in the plane of incidence (p wave) against that of a wave polarized perpendicular to the plane of incidence (s wave)<sup>30,31</sup>. Waveguide techniques based on the same principle have also been used and show fair agreement with the s-p reflection method<sup>32</sup>. Another approach is to detect the change in phase caused by electro-optic modulation with a conventional Mach Zehnder Interferometer (MZI)<sup>33,34,35</sup>. While the performance of this measurement is tedious and subject to the usual problems of interferometry, the data analysis is straightforward, and it is possible to measure the electro-optic coefficients, in our case  $r_{33}$  and  $r_{13}$ , directly, rather than simply measuring the ratio of the two and making assumptions to separate the factors.

### 4.2 Mach-Zehnder Interferometry

The Mach-Zehnder interferometer (See Fig. 4-1), invented over one hundred years ago, still finds numerous uses in optical experiments and measurements.

---

<sup>26</sup> W. H. G. Horsthuis and G. J. M. Krijnen, *Appl. Phys. Lett.* 55, 616 (1989).

<sup>27</sup> R. Meyrueix and G. Mignani, *Mater. Res. Soc. Symp. Proc. Ser. 173*, paper Q13.5 (1989).

<sup>28</sup> J. F. Valley, J. W. Wu, and C. L. Valencia, *Appl. Phys. Lett.* 57, 1084 (1990).

<sup>29</sup> S. Herminghaus, B. A. Smith, and J. D. Swalen, *J. Opt. Soc. Am. B* 8, 2311 (1991).

<sup>30</sup> C. C. Teng and H. T. Man, *Appl. Phys. Lett.* 56, 1734 (1990).

<sup>31</sup> R. N. Demartino, D. E. Allen, R. Keosian, G. Khanarian, and D. R. Haas, *Mater. Res. Soc. Symp. Proc.* 228, 39 (1992).

<sup>32</sup> R. A. Norwood, T. K. Findakly, H. A. Goldberg, G. Khanarian, J. B. Stamatoff, and H. N. Yoon, *Polymers for Lightwave and Integrated Optics: Technology and Applications*, edited by L. A. Hornak (Dekker, New York, 1992), Chap. 11.

<sup>33</sup> M. Sigelle and R. Hierle, *J. Appl. Phys.* 52, 4199 (1981).

<sup>34</sup> K. D. Singer, M. G. Kuzyk, W. R. Holland, J. E. Sohn, S. J. Lalama, R. B. Comizzoli, H. E. Katz, and M. L. Schilling, *Appl. Phys. Lett.* 53, 1800 (1988).

<sup>35</sup> R. A. Norwood, M. G. Kuzyk, and R. A. Keosian, *J. Appl. Phys.* 75 (4), 1869 (1994).

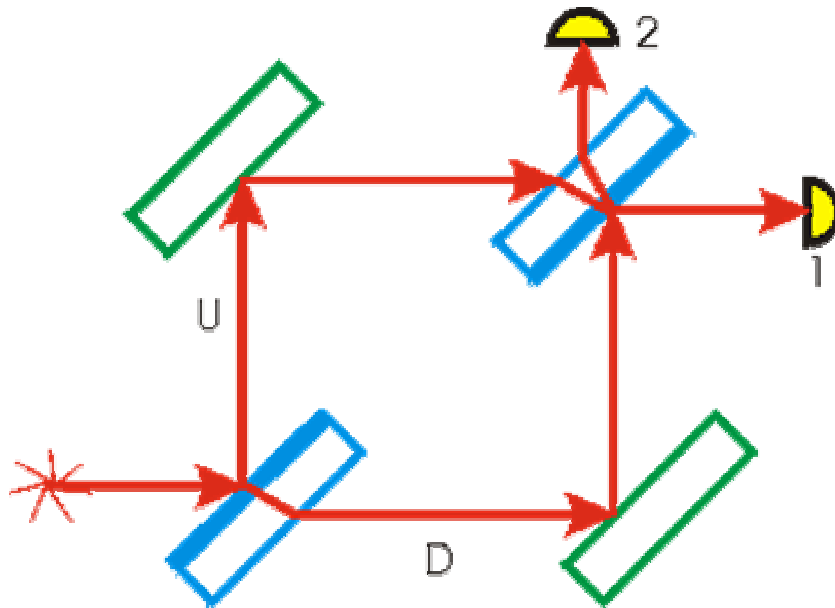


**Figure 4-1: Schematic representation of a MZI. Red-Optical radiation. Blue-Partially-silvered mirrors. Green-Mirrors. Yellow-Detectors.**

It can be intuitively understood that light incident upon the first partially-silvered mirror is split into two equal halves and that these halves travel separate paths. These paths, henceforth referred to as *signal* path and *reference* path are assumed to have equal optical path lengths. The second partially-silvered mirror acts like a summing junction, and upon incidence, the two beams interfere. If everything is aligned and the optical paths are indeed equal, the interference is constructive and the original beam is detected. If the phase of the *signal* arm is delayed, through some mechanism, by half a wavelength, the beams interference is said to be destructive and the output is nullified, thus resulting in no detected signal. If the same mechanism causes the phase in the *signal* path to be varied between 0 and  $\pi$  radians of delay, a sinusoidal signal is seen at the detector as the beam oscillates between constructive and destructive interference. Therefore, by measuring the intensity of the optical radiation at the detector, the phase in the *signal* path can be known at any given time. This is the basis of electro-optic interferometry.

### 4.3 Electro-Optic Interferometry

The MZI can be used to measure electro-optic phase modulation (See Fig. 4-2).

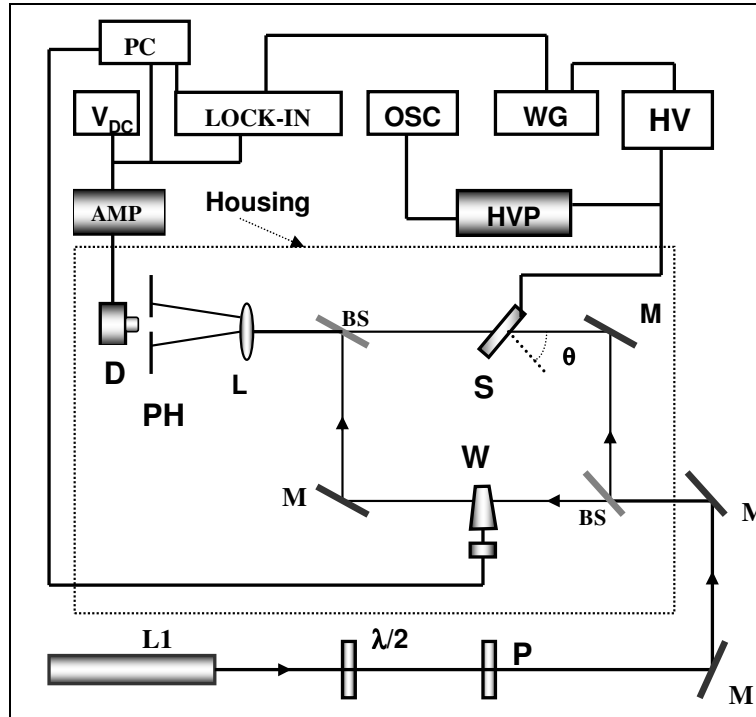


Figure 4-2: MZI. L1, He-Ne Laser (632.8 nm);  $\lambda/2$ , half-wave plate; P, polarizer; S, sample; D, silicon photodetector; AMP, amplifier;  $V_{dc}$ , multimeter; HVP, high-voltage probe; LOCK-IN, lock-in amplifier; OSC, oscilloscope; WG, waveform generator; HV, high-voltage amplifier; PC, computer; W, glass translation wedge; BS's, beamsplitters; M's, mirrors; PH, pin hole; L, lens.

In this configuration, the *reference* arm of the interferometer contains a glass wedge, which is slowly translated by a stepper motor to produce a controllable phase shift between the interfering beams and an electro-optic sample is mounted on a rotation stage in the *signal* arm. When an AC modulating voltage is applied to the tilted sample, a change in the refractive index, as well as a change in the path length, due to the change in the refraction angle, occurs. The resulting phase modulation in the *signal* beam is

$$\Delta\phi_{ac} = \frac{2\pi}{\lambda} (s \cdot \Delta n + n \cdot \Delta s), \quad (30)$$

where  $\lambda$  is the optical wavelength,  $n$  is the refractive index of the material, and  $s$  is the optical path length given by

$$s = d / \cos \alpha; \quad (31)$$

here  $d$  stands for the thickness of the sample and  $\alpha$  is the refraction angle<sup>36</sup>. This phase shift causes a modulation of the light intensity exiting the interferometer, which can be expressed as

$$\Delta\phi_{ac} = 2\sqrt{2} \frac{I_{ac,rms}}{I_{\max} - I_{\min}}. \quad (32)$$

Here  $I_{ac,rms}$  is the modulated intensity due to the AC electric field; and  $I_{\max}$  and  $I_{\min}$  are the maximum and the minimum intensities resulting from a  $\pi$  phase shift of the reference beam due to wedge translation.

For the case of  $s$ -polarized light obliquely illuminating the sample, a general formula for the  $r_{13}$  coefficient of the material can be determined from the previous equations with the approximation that  $n_e \approx n_o = n$ ; it is given as

$$r_{13} = \frac{2\lambda}{\pi n V_{ac,rms}} \frac{I_{ac,rms}}{I_{\max} - I_{\min}} \frac{(1 - \sin^2 \theta / n^2)^{3/2}}{n^2 - 2 \sin^2 \theta}. \quad (33)$$

Here,  $V_{ac,rms}$  is the modulating voltage applied to the sample and  $\theta$  is the external angle of incidence of the *signal* beam on the sample. For  $p$  polarization of the laser light, we use

$$\sin^2 \alpha / n_e^2 + \cos^2 \alpha / n_o^2 = 1 / n_p^2, \quad (34)$$

where  $\alpha$  is the refraction angle of the beam inside the film, to obtain the expression relating the coefficients  $r_{13}$  and  $r_{33}$  as

---

<sup>36</sup> B. Swedek, N. Cheng, Y. Cui, J. Zieba, J. Winiarz, and P. Prasad, J. Appl. Phys. 82 (12), 5923 (1997).

$$r_{33} \sin^2 \alpha + r_{13} \cos^2 \alpha = \frac{2\lambda}{\pi n V_{ac,rms}} \frac{I_{ac,rms}}{I_{\max} - I_{\min}} \frac{(1 - \sin^2 \theta / n^2)^{3/2}}{n^2 - 2 \sin^2 \theta}. \quad (35)$$

Therefore, by measuring the modulation for both light polarizations, one can obtain values for  $r_{33}$  and  $r_{13}$ .

## 5. Experiment Description

### 5.1 Introduction

This chapter includes a description of the experiment performed. This experiment, it is important to recall, is designed to test the author's hypothesis that self-assembled films, having an intrinsic dipolar molecular orientation, will necessarily have enhanced non-linear optical characteristics compared to that of like polymers that were deposited with other, non-self-assembled techniques. To this end, samples of two types of polymers, Poly S-119 and CLD-1, known to have non-linear optical properties, were prepared and their electro-optic coefficients determined.

### 5.2 Poly S-119

Poly S-119 (henceforth referred to as PS-119) is a commercially available polymer that is known to have non-linear optical properties and was purchased from Sigma. Poly diallyl dimethyl ammonium chloride (PDDA) is commercially available and was purchased from Aldrich. Five samples of PS-119/PDDA were fabricated with the ESA method.

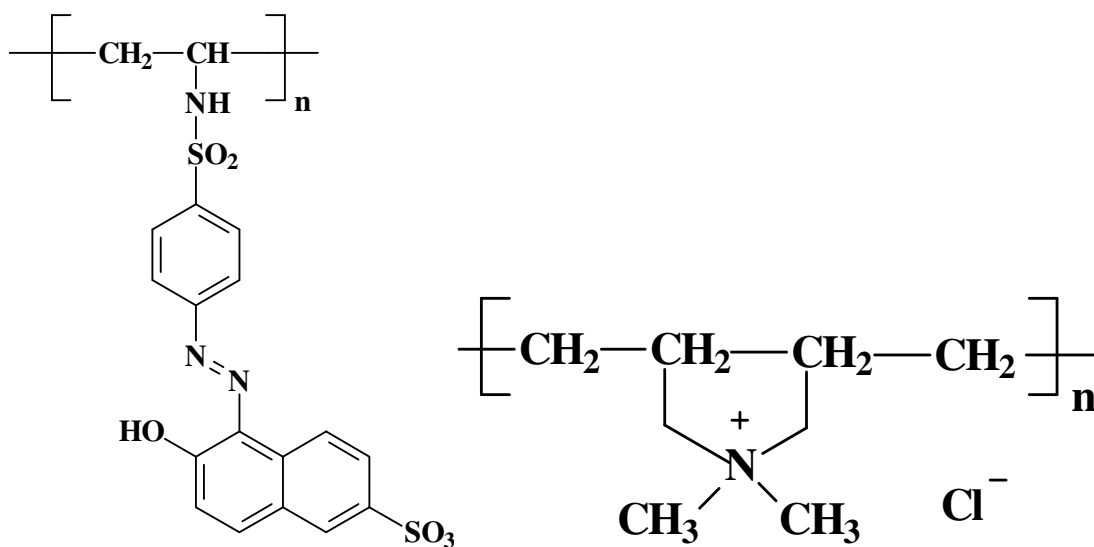


Figure 5-1: Left-PS-119 molecular structure. Right-PDDA molecular structure.

ITO-coated glass substrates were cleaned thoroughly using a solution of acetone and isopropyl alcohol, then rinsed extensively with ultra-pure water. The substrate was first immersed in a cationic 1% PDDA (v/v) aqueous solution for 1 minute, and then rinsed extensively in ultra-pure water, forming a monolayer of PDDA molecules. Immersion in an anionic aqueous solution of PS-119 with a concentration of 2 mg/ml for 1 minute, again followed by thorough rinsing in ultra-pure water, produced a uniform PS-119 monolayer on the top film surface. Subsequent bilayers were added by repetition of this alternating two-step process, until the desired number of bilayers was achieved.

### 5.3 CLD-1

CLD-1 is a ring-locked, phenyltetraene-based, second-order nonlinear optical chromophore designed by Larry Dalton *et al.*<sup>37,38,39,40</sup> for the explicit purpose of electro-optic device fabrication.

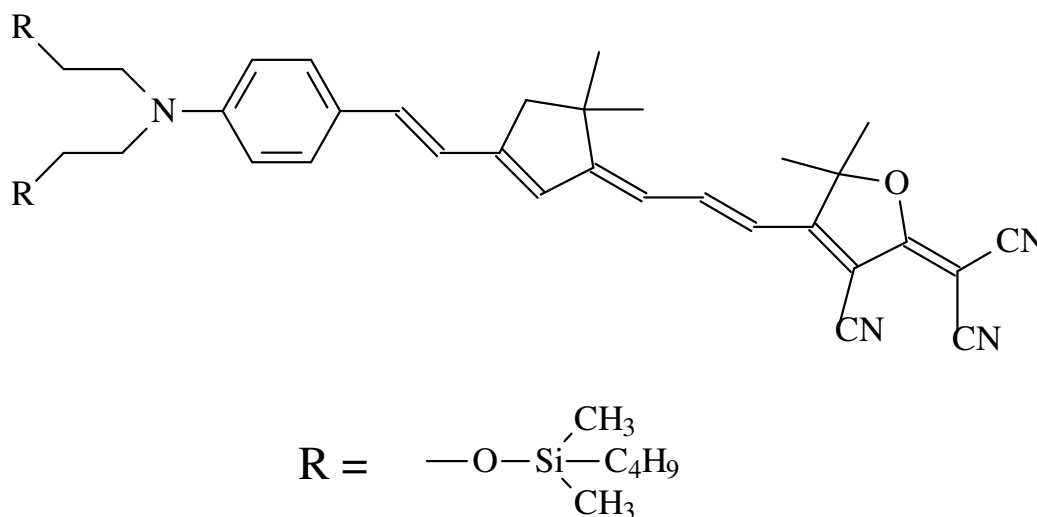


Figure 5-2: The molecular structure of CLD-1.

<sup>37</sup> C. Zhang, A. S. Ren, F. Wang, L. R. Dalton, S. S. Lee, S. M. Garner, and W. H. Steier, Polym. Prepr. (Am. Chem. Soc. Div. Polym. Chem.) 40, 49 (1999).

<sup>38</sup> Y. Shi, C. Zhang, H. Zhang, J. H. Bechtel, L. R. Dalton, B. H. Robinson, and W. H. Steier, Science 288, 119 (2000).

<sup>39</sup> Y. Shi, W. Lin, D. J. Olson, J. H. Bechtel, H. Zhang, W. H. Steier, C. Zhang, and L. R. Dalton, Appl. Phys. Lett. 77 (1), 1 (2000).

<sup>40</sup> C. Zhang, M. C. Oh, H. Zhang, W. H. Steier, and L. R. Dalton, Chem. Mater. 13, 3043 (2001).

CLD-1 was provided by the Dalton group through an agreement with Wright Patterson Air Force Base. Because of the limited amount obtained, only one sample of CLD-1/PDDA was fabricated by the ESA method and one spin-coated sample, to use as a comparison.

In order to self-assemble a CLD-1/PDDA multi-layer structure, it was necessary to modify CLD-1 slightly by treating it with sulfuric acid to form water soluble sulfonated CLD-1. After this modification, a deposition process that is similar to that used for the PS-119 samples was performed. ITO-coated glass substrates were cleaned thoroughly using a solution of acetone and isopropyl alcohol, then rinsed extensively with ultra-pure water. The substrate was first immersed in a cationic 1% PDDA (v/v) aqueous solution for 1 minute, and then rinsed extensively in ultra-pure water, forming a monolayer of PDDA molecules. Immersion in an anionic aqueous solution of CLD-1 with a concentration of 2 mg/ml for 1 minute, again followed by thorough rinsing in ultra-pure water, produced a uniform CLD-1 monolayer on the top film surface. Subsequent bilayers were added by repetition of this alternating two-step process, until the desired number of bilayers was achieved.

For comparison, a spin-coated sample of CLD-1 was fabricated. The film was poled by first heating it to 103 °C and then applying a 120 V electric field. The film was kept under these conditions for approximately one hour and then left to cool to room temperature, while the electric field was maintained, for approximately one hour. This poling process is needed to ‘freeze’ the alignment of the chromophores.

#### **5.4 Control Sample**

A control sample was fabricated to ensure the validity of the measurements. This sample, Control-1, was made with 5CB and polymethyl methacrylate ( $M_w = 120,000$ , from Aldrich) with a ratio of 2 to 1 using Chloroform and acetone (1: 2 V/V) as solvents. The thickness of Control-1 was determined, by using a Rudolph Research AutoELR-II ellipsometer, to be 1 micron. This control sample, which was fabricated by spin-coating on ITO coated glass, contains no non-linear optical material.

## 5.5 Sample Preparation

The electro-optic samples were prepared by placing the film between two ITO-coated glass electrodes. The film is already deposited on an ITO coated glass substrate, which will serve as a grounding plane, the other piece of ITO coated glass will serve as the ‘hot’ electrode and is oriented orthogonal to the glass that the film is on, in such a way as to form a ‘T’ shape. This is to facilitate the mounting of the sample in the interferometer. Since the film is so thin, a Harrick model MSP-006 6  $\mu\text{m}$  thick teflon spacer with an inner diameter of 25 mm is placed between the film and the ‘hot’ electrode to prevent electrical shorts from forming. Optical adhesive, a clear (See Fig. 5-3), colorless, liquid photopolymer requiring UV curing, is used to seal the ‘T’ sample at the interfaces and hold the ITO electrodes in place. NORLAND optical adhesive #63 (“NOA63”) was used and was cured with a RAYTECH ultra-violet curing lamp with a wavelength of 365 nm for approximately five minutes. This adhesive had an index of refraction of 1.56 after curing. After curing, copper tape was applied to both electrodes respectively, to facilitate the attachment of probes. The copper tape was then covered with electrical tape (See Fig. 5-4).

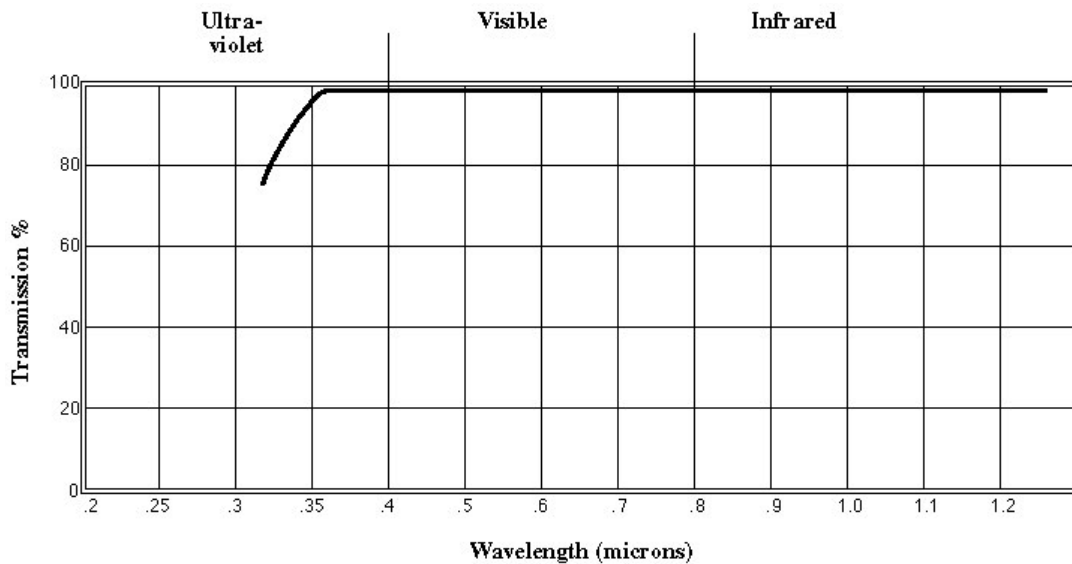
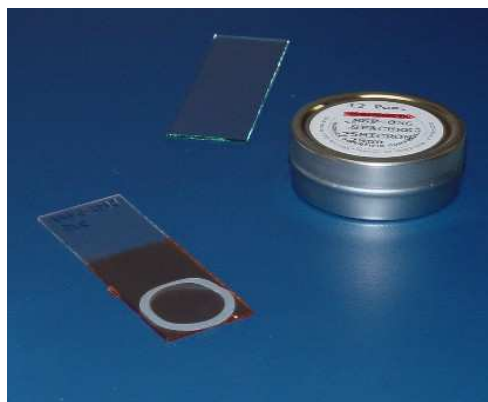


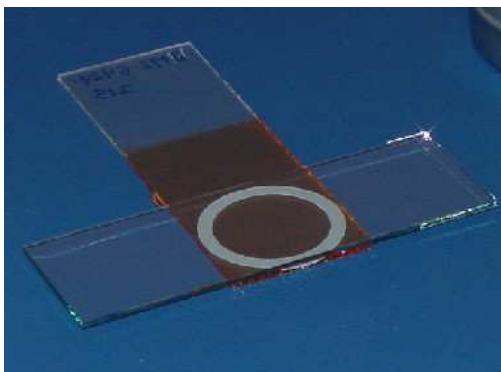
Figure 5-3: Spectral transmission characteristics of NOA63.



Step 1: Required equipment/hardware for sample preparation.



Step 2: Position spacer on top of EO film.



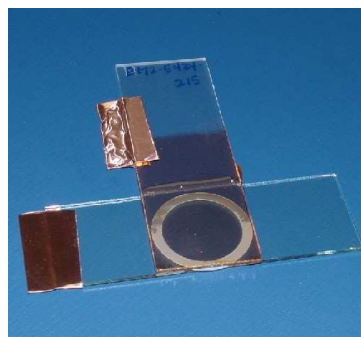
Step 3: Position another ITO coated slide on top of spacer (conductive side down).



Step 4: Deposit optical glue at the interface and let seep through to spacer.



Step 5: Cure glue with 365 nm UV lamp for 5 minutes.



Step 6: Apply copper tape.

Figure 5-4: Preparing the samples for measurement.

## **5.6 The Measurement**

The MZI was set-up on a vibration-isolated optical table and is shown in figure 5-5. In addition, a poly-carbonate housing was used to reduce the influence of air fluctuations on the stability of the interferometer. For a conceptual schematic of the measurement scheme, see figure 4-2 of the previous chapter.

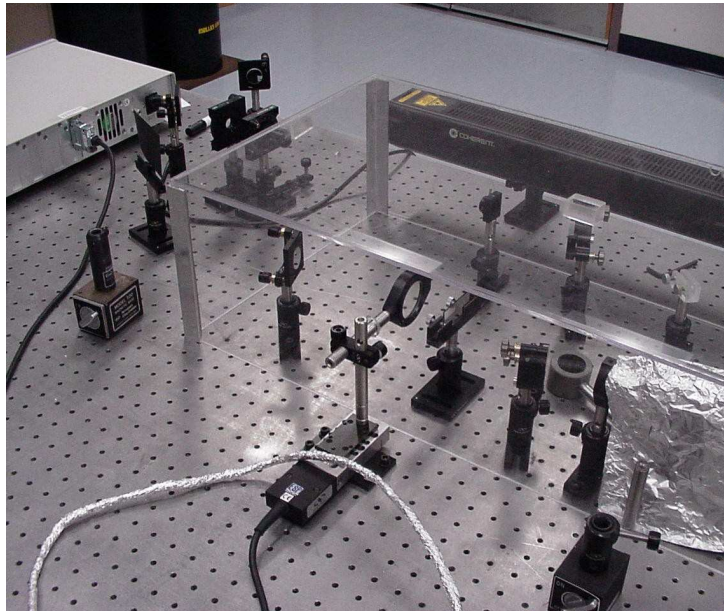


**Figure 5-5: The MZI.**

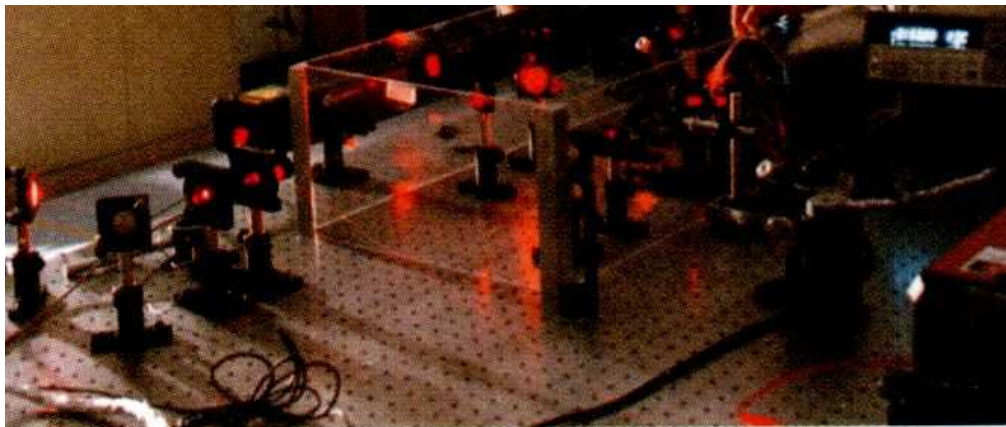


**Figure 5-6: The MZI in action.**

The prepared samples were mounted on a rotating stage in the *signal* arm of the MZI at  $45^\circ$  to the normal and were illuminated by a Melles Griot model 05-LHP-111 5 mW HeNe laser with  $\lambda = 632.8$  nm. The samples were measured in transmission with the optical field propagating perpendicular to the plane of film. A Stanford Research Systems model DS345 30 MHz synthesized function generator was used to supply an input sinusoidal signal which was in turn amplified by a TREK model 610D high power amplifier. This AC signal was sent to the EO sample and was applied parallel to the plane of optical propagation. The actual voltage applied to the sample was measured with a Tektronix model TDS210 digital oscilloscope in conjunction with a Tektronix model P6105 passive high voltage probe. A Newport universal motion controller/driver model ESP300 was used to translate the glass wedge, which produces a slow, controllable phase shift in the *reference* arm of the interferometer.

The output signal was detected by a UDT Pin 10 silicon photodetector operating in the photovoltaic mode. This signal, in turn, was amplified by a UDT Tramp transimpedance amplifier operating in the current-to-voltage mode. This is an instrument which provides low input impedance to accurately measure the short circuit current of phototransducers such as silicon and germanium photodetectors. This signal is split and sent to a HP model 34401A digital multimeter and a Stanford Research System SRS850 DSP lock-in amplifier, respectively. The digital multimeter allows for the intensity of the optical carrier at the interferometer's output to be observed, while the lock-in amplifier allows the considerably smaller modulated signal to be detected. The AC signal from the function generator is split and sent to the lock-in amplifier to serve as a reference.

For each sample, it was necessary to precision align the interferometer before measurement. Sinusoidal waveforms of varying frequencies were produced with the function generator and, after amplification, applied across the electro-optic sample. For each frequency, the voltage applied to the EO sample was recorded as well as the magnitude of the detected modulation signal from the lock-in amplifier. The maximum and minimum intensities of the optical carrier, as induced by the relatively slow translation of the glass wedge in the *reference* arm of the interferometer, were displayed

on the digital multimeter and recorded. Because of drift of the interferometers alignment it could not be assumed that these values were constant throughout the measurement process. Therefore, it was necessary to record these maximum and minimum intensities for every third frequency measured. This multi-frequency measurement process was performed for both s and p wave polarizations on all samples. For each experimental data point, measurements were collected for 200 seconds and an average was taken.

To ensure the settling of the lock-in before data acquisition, the time constant of its RC filter was set according to the following relationship:

$$\tau \approx 5 \times \frac{1}{f}. \quad (36)$$

Where  $\tau$  is the time constant and  $f$  is the frequency of the sinusoidal waveform modulating the EO sample. The highest measured modulating frequency, 7 kHz, was limited by the bandwidth of the high voltage amplifier supplying the modulating voltage.

To further reduce the noise contribution to the system, an electro-magnetic shield consisting of 2/1000 inch thick  $\mu$ -metal from Magnetic Shield Corporation was constructed for the high voltage amplifier. The systems cables and detector were shielded with regular aluminum foil.

### 6.1 Introduction

This chapter summarizes the results of the experiments described in the previous chapter. These results include data from the control sample, the five PS-119 ESA fabricated samples, the CLD-1 ESA fabricated sample, and the CLD-1 spin-coated sample. Note that, where given, sample thickness and index of refraction data were taken with a Rudolph Research AutoELR-II ellipsometer.

### 6.2 Separating the ‘True’ Electronic Contribution

At this point it is necessary to clarify terminology. When the modulating AC electric field is applied, a periodic changing of the degree of orientation of the chromophores occurs. When the applied field changes over time, the chromophores will tend to change their degree of orientation to the total field, consequently changing the materials birefringence. At low frequencies, the modulation of the birefringence contributes to the modulation of the refractive index. At high frequencies, the inertia of the rod-like chromophores prevents them from changing their degree of orientation to follow the AC field. Hence, at high frequencies, the birefringence is not modulated and does not provide the additional modulation to the refractive index observed at low frequencies. The high frequency cutoff will depend on the viscosity of the surrounding media and the volume of the chromophores.

Including linear, second-, and third-order non-linear effects, the refractive index changes induced in a low  $T_g$  polymer by an applied electric field can be written as

$$\Delta n_{o,e} = \frac{2\pi}{n} (S^2 B_{o,e} + 2SC_{o,e} E_T + 3D_{o,e} E_T^2), \quad (37)$$

where  $o$  and  $e$  refer to the *ordinary* and *extraordinary* waves, respectively,  $S$  is a scaling factor necessary to take into account the fact that a poling field is unnecessary to achieve

chromophore alignment when fabrication of films is done with the ESA method, and  $E_T$  is the total electric field and is equal to

$$E_T = E_B + E_{AC}. \quad (38)$$

$E_B$  is the DC bias field and is zero in this experiment, and the B, C and D coefficients are related to the microscopic properties of the chromophores and to the local field correction factors that take into account the dielectric effects of the surrounding matrix<sup>41,42,43</sup>.

The first term on the right hand side of the above equation describes the birefringence induced by the orientation of the chromophores. The second term accounts for the linear EO effect (a.k.a. Pockel's effect, this is what is referred to as the 'true' electronic contribution). The third term describes the Kerr effect (a.k.a. quadratic electro-optic effect), which is proportional to the square of the total field.

As there are three different modulating mechanisms it is perhaps inappropriate to characterize an electro-optic coefficient if no attempt is made to separate the three. It has therefore been assumed that contribution of birefringence above 1 kHz is negligible. Furthermore, it has been assumed that the contribution from the Kerr effect is also negligible. Therefore, this author shall refer to the films *responsivity* (R) when discussing the total response with the understanding that it is assumed that the responsivity at high frequencies (i.e.  $>1$  kHz) will simplify down to the 'true' electronic contribution of the electro-optic effect.

It is important to note that, while it is interesting to observe the electro-optic coefficients at multiple frequencies, it is generally assumed that the true electronic contribution will

---

<sup>41</sup> J. W. Wu, J. Opt. Soc. B 8, 142 (1991).

<sup>42</sup> B. Kippelen, K. Sandalphon, K. Meerholz, and N. Peyghambarian, Appl. Phys. Lett. 68 (13), 1748 (1996).

<sup>43</sup> B. Kippelen, K. Sandalphon, K. Meerholz, and N. Peyghambarian, Appl. Opt. 35 (14), 2346 (1996).

have a flat response from DC to many hundreds of GHz<sup>44,45</sup>. Any frequency dependence probably implies the presence of other factors.

### 6.3 Sample Data

Figure 6-1 provides an illustration of the data collected for each sample.

Polarization	Modulated Frequency (Hz)	I <sub>max</sub> (mV)	I <sub>min</sub> (mV)	Applied Voltage (V pk-pk)	Modulated Signal Intensity (μV)
S	10	205	84	136	23
S	30	205	84	140	5
S	50	205	84	144	3
S	70	204	81	144	1.7
S	100	204	81	144	1
S	300	204	81	144	0.5
S	500	205	80	144	0.25
S	700	205	80	144	0.25
S	1000	205	80	146	0.21
S	3000	204	89	144	0.18
S	5000	204	89	144	0.18
S	7000	204	89	140	0.18
P	10	208	110	144	12.4
P	30	208	110	142	3
P	50	208	110	146	1.9
P	70	208	106	146	0.7
P	100	208	106	147	0.57
P	300	208	106	146	0.5
P	500	208	108	146	0.15
P	700	208	108	147	0.14
P	1000	208	108	147	0.13
P	3000	207	110	146	0.13
P	5000	207	110	144	0.13
P	7000	207	110	144	0.13

**Figure 6-1: An example of the data collected.**

<sup>44</sup> C. Zhang, M. C. Oh, H. Zhang, W. H. Steier, and L. R. Dalton, Chem. Mater. 13, 3043 (2001).

<sup>45</sup> D. A. Kleinman, Phys. Rev. 126 (6), 1977 (1962).

## 6.4 Effective Voltage

As the applied electric field is dropped across the entire sample 'sandwich', it is necessary to calculate an effective voltage in order to calculate the electro-optic coefficients. To this end, it was assumed that the air gap and the film behave as two dielectrics in series.

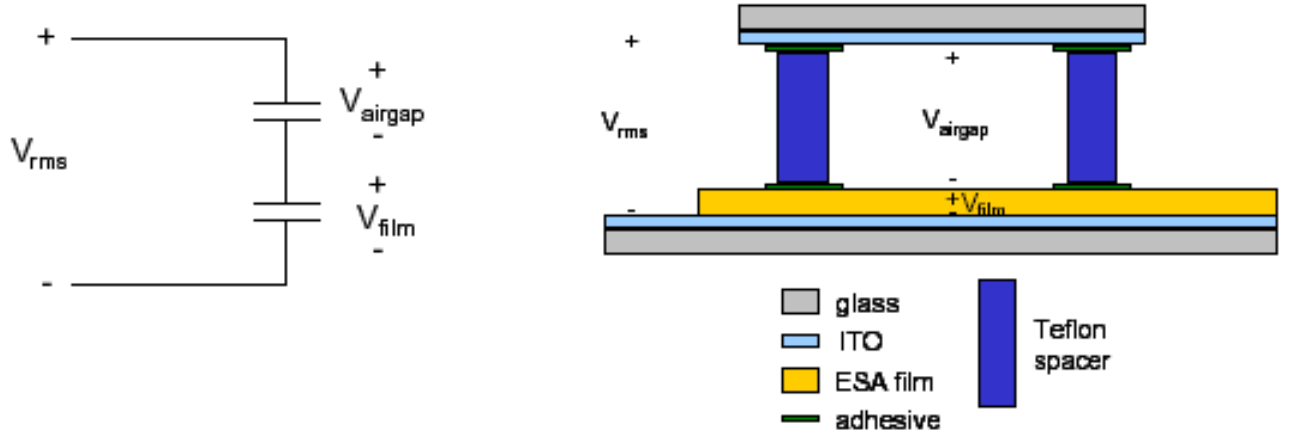


Figure 6-2: Model of the sample 'sandwich'.

Assuming

$$A_{airgap} = A_{film} = A \quad (39)$$

$$C_{film} = \frac{\epsilon_{film} \epsilon_o A}{t_{film}} \quad (40)$$

$$C_{airgap} = \frac{\epsilon_{airgap} \epsilon_o A}{t_{airgap}}, \quad (41)$$

where A is the area,  $\epsilon$  is the dielectric constant of the material,  $\epsilon_o$  is the permittivity of a vacuum, C is the capacitance, and t is the thickness. Then

$$V_{eff} = V_{film} = \frac{q}{C_{film}} = q \frac{t_{film}}{\epsilon_{film} \epsilon_o A} \quad (42)$$

$$V_{rms} = V_{airgap} + V_{film} = q \left( \frac{1}{C_{airgap}} + \frac{1}{C_{film}} \right) = q \left( \frac{t_{airgap}}{\epsilon_{airgap} \epsilon_o A} + \frac{t_{film}}{\epsilon_{film} \epsilon_o A} \right) \quad (43)$$

$$\frac{V_{film}}{V_{rms}} = \frac{q \frac{t_{film}}{\epsilon_{film} \epsilon_o A}}{q \left( \frac{t_{airgap}}{\epsilon_{airgap} \epsilon_o A} + \frac{t_{film}}{\epsilon_{film} \epsilon_o A} \right)} = \frac{\frac{t_{film}}{\epsilon_{film}}}{\frac{t_{airgap}}{\epsilon_{airgap}} + \frac{t_{film}}{\epsilon_{film}}} = \frac{\epsilon_{airgap} t_{film}}{\epsilon_{film} t_{airgap} + \epsilon_{airgap} t_{film}}. \quad (44)$$

And assuming

$$\epsilon_{airgap} \approx 1 \quad (45)$$

and

$$\epsilon_{film} \approx n_{film}^2, \quad (46)$$

Then

$$V_{eff} = V_{film} = \frac{t_{film}}{n_{film}^2 t_{airgap} + t_{film}} V_{rms} \quad (47)$$

## 6.5 Error of MZI Measurement

Through trial and error, the experimental error of this measurement was determined to be within 7.5%.

## 6.6 Results from Control Sample

The sample Control-1 was measured and the electro-optic coefficients were calculated to be  $r_{13} = 0.151 \text{ pm/V}$  and  $r_{33} = 1.36 \text{ pm/V}$  at 1 kHz. These values are small, but non-zero.

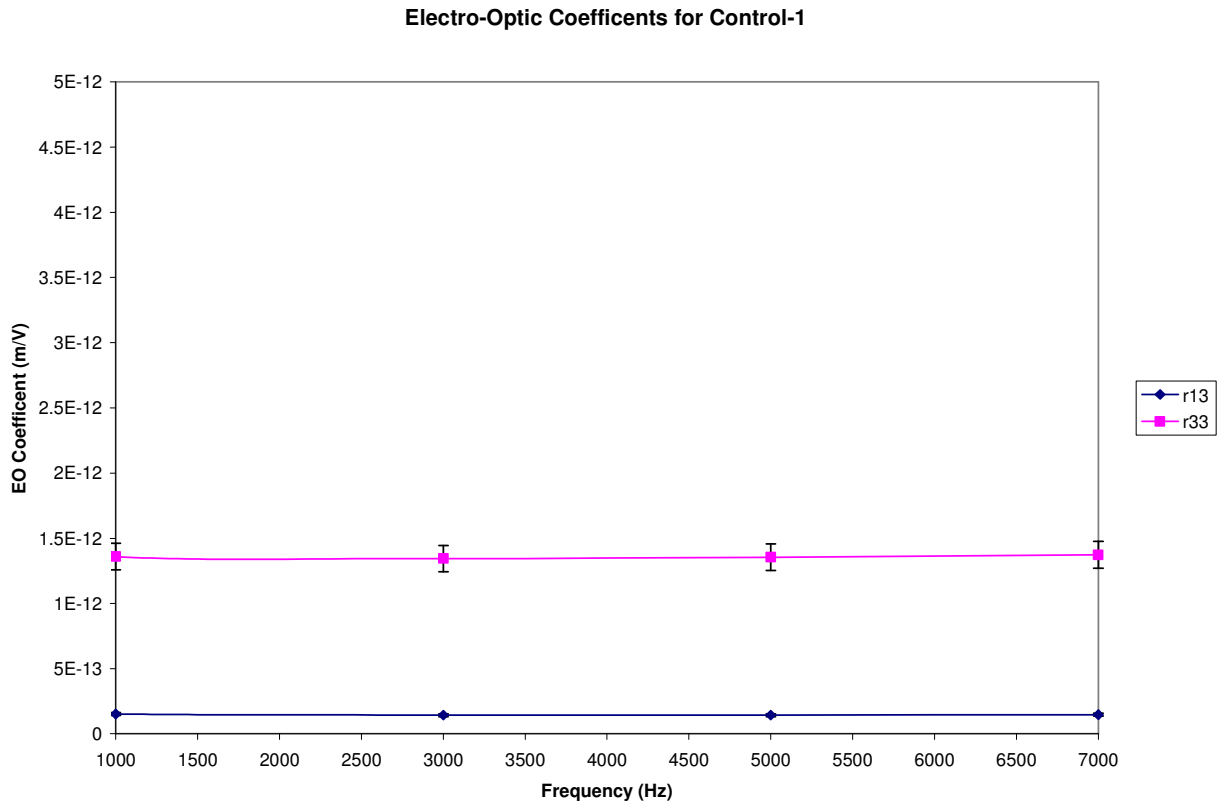


Figure 6-3: Electro-optic coefficients of Control-1.

## 6.7 Results from PS-119

Sample #	Index of refraction (n)	Thickness (nm)	$r_{33}$ (pm/V)	$r_{13}$ (pm/V)
1	1.67	90	17.5	1.3
2	1.67	90	12.6	1.2
3	1.68	130	13.6	1.0
4	1.62	60	16.1	1.8
5	1.51	60	30.8	1.7

Figure 6-4: Summary of PS-119 data. EO coefficient values are taken at 1 kHz.

r33 of PS-119 Samples

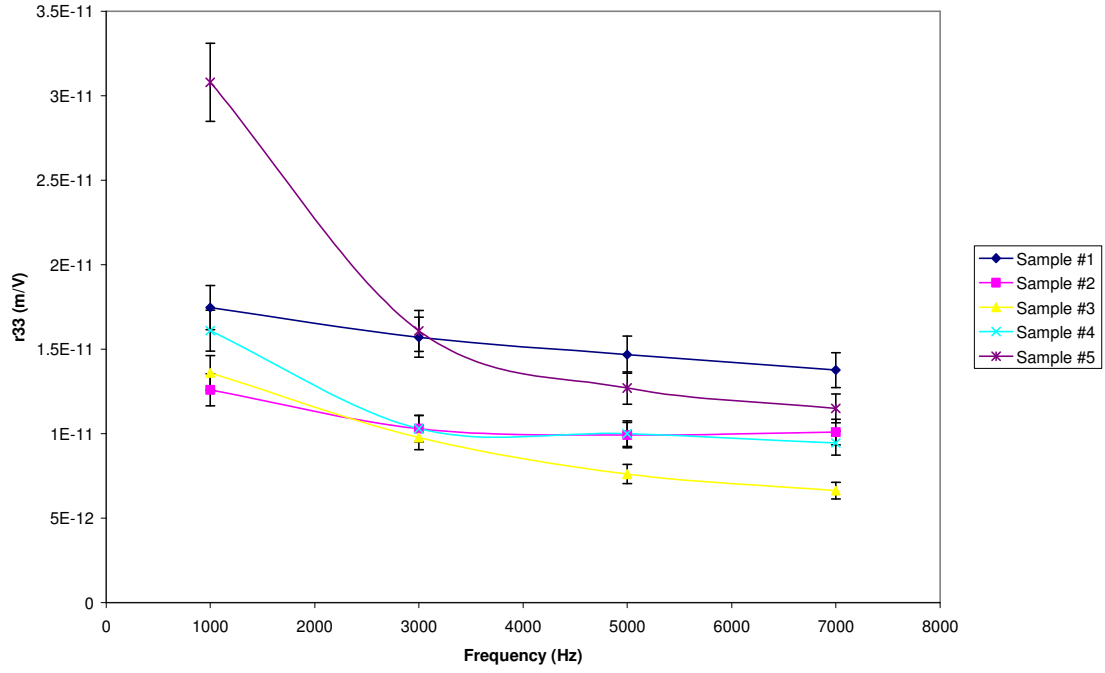


Figure 6-5: r33 of PS-119 samples.

r13 of PS-119 Samples

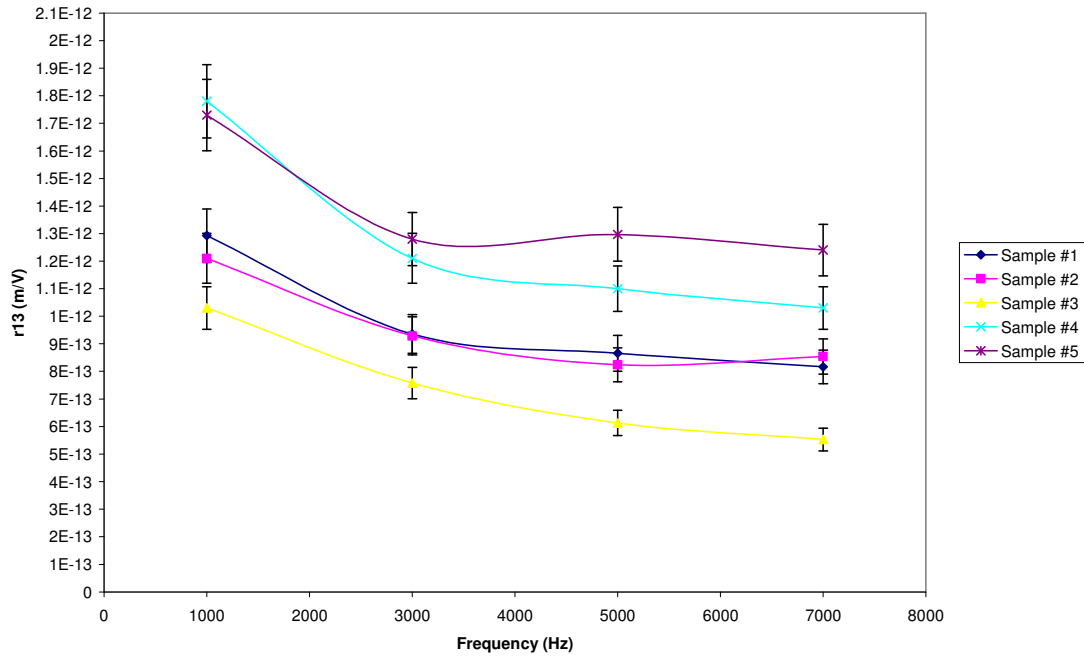


Figure 6-6: r13 of PS-119 samples.

## 6.8 Results from CLD-1

The ESA fabricated and spin-coated samples of CLD-1 were measured and the electro-optic coefficients were calculated to be  $r_{13} = 2.6$  pm/V and  $r_{33} = 28.9$  pm/V, and  $r_{13} = 1.4$  pm/V and  $r_{33} = 10.4$  pm/V at 1 kHz, respectively.

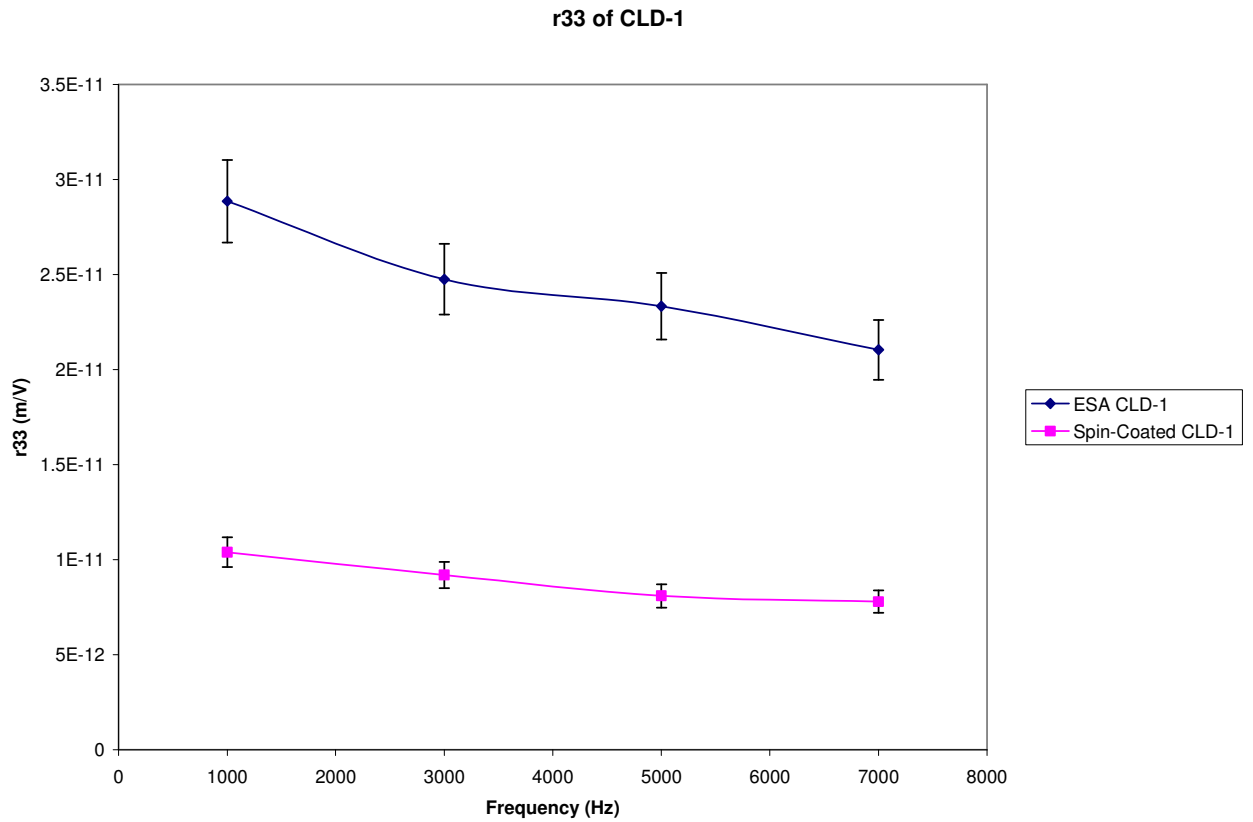
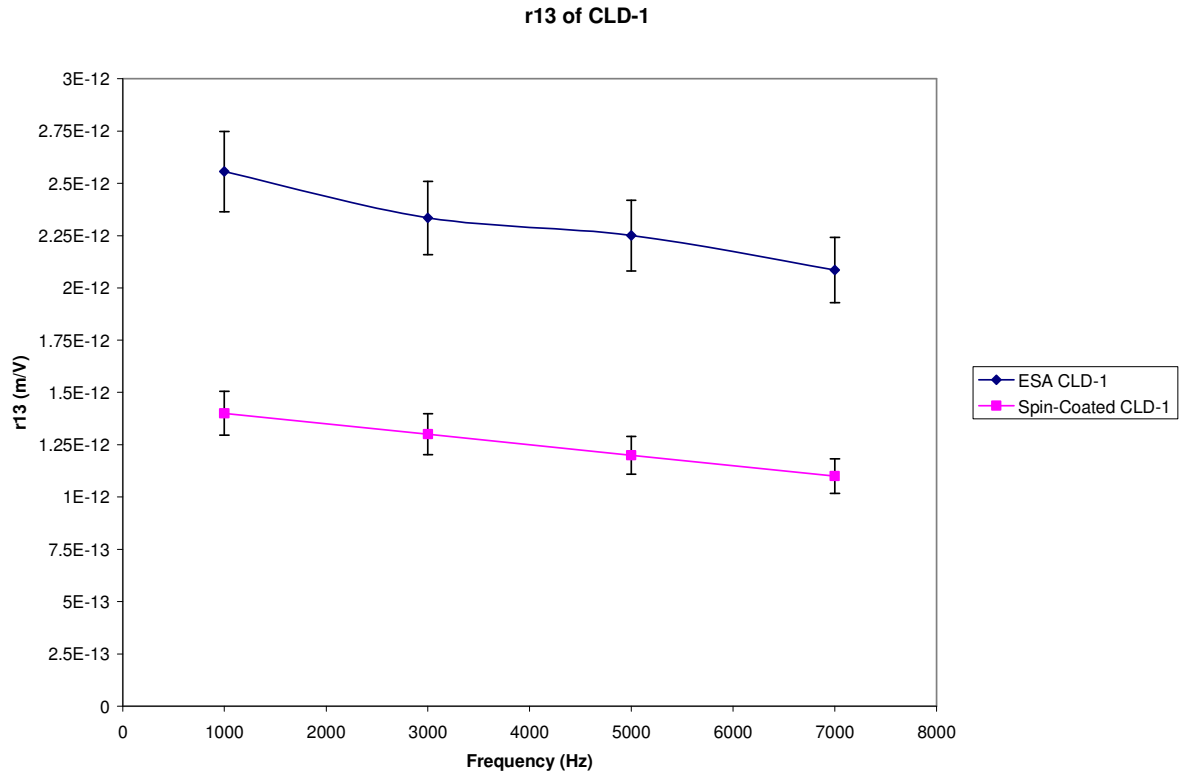


Figure 6-7:  $r_{33}$  of CLD-1.



**Figure 6-8: r13 of CLD-1.**

### ***6.9 Birefringence Contribution***

Figures 6-9 and 6-10 show the Responsivity of the ESA fabricated CLD-1 sample. This serves as a clear example of the birefringence contribution.

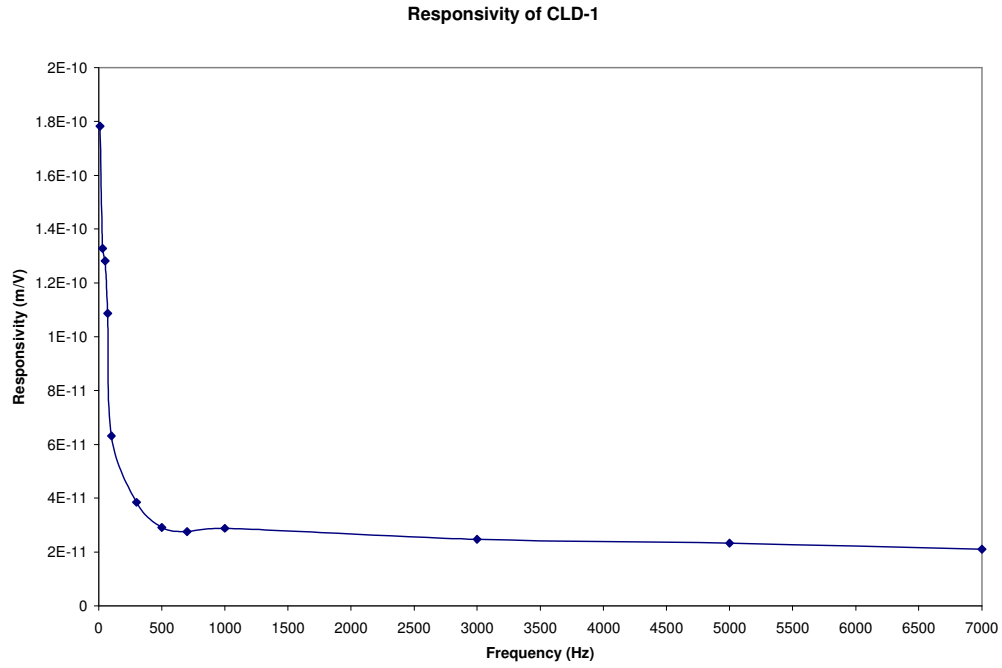


**Figure 6-9: Responsivity of ESA fabricated CLD-1.**

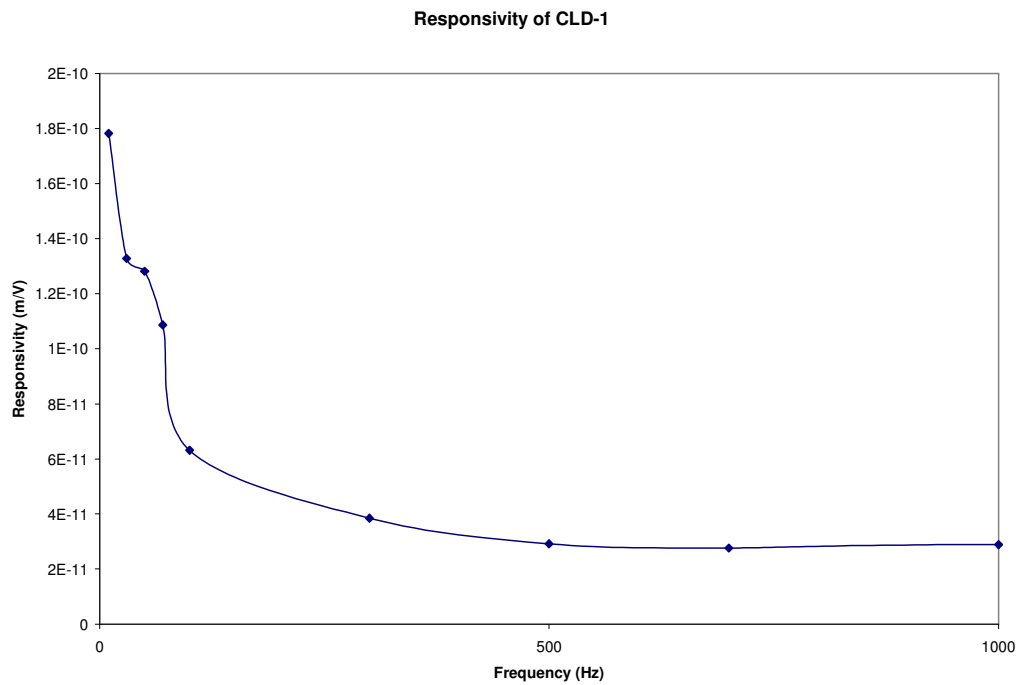


**Figure 6-10: Responsivity of ESA fabricated CLD-1. Birefringence contribution is obvious at very low frequencies but quickly dies out.**

### ***7.1 Frequency Dependence***

It can be seen from the results in the previous chapter that no relevant frequency dependence can be seen in the control sample. However, the ESA fabricated PS-119 films displayed a fairly strong frequency dependence in the range of interest. Particularly telling is the CLD-1 data. A small frequency dependence can be seen in the spin-coated sample, whereas the ESA fabricated sample shows significant frequency dependence. This author can only speculate that the nature of the polar order in the ESA films allows the birefringence to make contributions to the responsivity at greater frequencies than anticipated.

### ***7.2 ESA vs. Spin-Coated EO Coefficients for CLD-1***

As can be seen, the ESA fabricated sample of CLD-1 has an  $r_{33}$  EO coefficient that is approximately 178% greater than that of the spin-coated sample, and an  $r_{13}$  EO coefficient that is approximately 85% greater. This result would seem to support the author's contention of an enhanced polar order in self-assembled polymers over that of poled polymers.

### ***7.3 Differences in Similar ESA Fabricated Films***

Despite being fabricated with similar properties, two of the ESA fabricated films show significant differences in EO coefficients. PS-119 samples #1 and #2 were fabricated to be identical. However, there is a 28% drop in the  $r_{33}$  coefficient and a 7.5% drop in the  $r_{13}$  from sample #1 to sample #2 at 1 kHz. This author can only conclude that other factors, primarily ESA fabrication factors such as dip and rinse time, are responsible for this result.

## **7.4 Suggestions for Future Work**

While the results contained herein are interesting, the author acknowledges that such a small sample set does not represent a complete statistically valid basis for a new paradigm in polymer EO modulator fabrication. It does, however, lay the ground work for future endeavors. Further study of the frequency dependence with the ability to probe the higher frequencies would be very useful and interesting. The author suggests that further study of the ESA fabrication variables would be prudent. Furthermore, this author suggests that the fabrication of an EO ESA polymer modulator would give a better feel for where the trouble areas lay, and could serve as a sufficient demonstration of the potential of this area of research.

## **7.5 Conclusion**

Electrostatic self-assembled polymer films having non-linear optical chromophores have been fabricated and have been determined to display significant optical non-linearity. The  $r_{33}$  EO coefficients have been demonstrated to be on the order of that of  $\text{LiNbO}_3$  ( $\approx 30.8$  pm/V). These results compare very favorably with the best poled polymers and indicate that the first requirement for the replacement of poled polymers in commercial devices has been met.

## REFERENCES

1. S. J. Lalama, and A. F. Garito, Phys. Rev. A 20, 1179 (1979).
2. Y. G. Zhao, A. Wu, H. L. Lu, S. Chang, W. K. Lu, S. T. Ho, M. E. van der Boom, and T. J. Marks, Appl. Phys. Lett. 79 (5), 589 (2001).
3. C. Zhang, M. C. Oh, H. Zhang, W. H. Steier, and L. R. Dalton, Chem. Mater. 13, 3043 (2001).
4. D. Chen, H. R. Fetterman, A. Chen, W. H. Steier, L. R. Dalton, W. Wang, and Y. Shi, Appl. Phys. Lett. 70, 3335 (1997).
5. Y. Shi, W. Lin, D. J. Olson, J. H. Bechtel, H. Zhang, W. H. Steier, C. Zhang, and L. R. Dalton, Appl. Phys. Lett. 77, 1 (2000).
6. Y. Shi, C. Zhang, H. Zhang, J. H. Bechtel, L. R. Dalton, B. H. Robinson, and W. H. Steier, Science 288, 119 (2000).
7. D. Chen, H. R. Fetterman, A. Chen, W. H. Steier, L. R. Dalton, W. Wang, and Y. Shi, Appl. Phys. Lett. 70, 3335 (1997).
8. E. Riande, E. Saiz, *Dipole Moments and Birefringence of Polymers*, edited by J. E. Marks, Prentice Hall, Englewood Cliffs, New Jersey 1992.
9. G. R. Fowles, *Introduction to Modern Optics*, Dover Publications, Inc., New York 1989.
10. *Polymers for Second-Order Nonlinear Optics*, edited by G. A. Lindsay and K. D. Singer, American Chemical Society, Washington, D. C. 1995.
11. K. D. Singer, M. G. Kuzyk, and J. E. Sohn, J. Opt. Soc. Am. B 4 (6), 968 (1987).
12. P. N. Prasad, D. J. Williams, *Introduction to Nonlinear Optical Effects in Molecules and Polymers*, John Wiley & Sons, Inc. 1991.
13. *Nonlinear Optical Properties of Organic and Polymeric Materials*, edited by D. J. Williams, American Chemical Society, Washington, D. C. 1983.
14. M. A. Karim, *Electro-Optical Devices and Systems*, edited by J. Plant, PWS-Kent Publishing Company, Boston, Massachusetts, 1990.
15. D. Chen, "High Speed Polymer Modulators", Ph.D. dissertation, Electrical Engineering Dept., University of California, Los Angeles, 1997.
16. *Polymers for Second-Order Nonlinear Optics*, edited by G. A. Lindsay and K. D. Singer, American Chemical Society, Washington, D. C. 1995.
17. Y. J. Liu, A. Wang, and R. O. Claus, Appl. Phys. Lett. 71 (16), 2265 (1997).
18. L. M. Zhang, F. Zhang, K. Cooper, Y. X. Wang, Y. J. Liu, and R. O. Claus, Opt. Comm. 186, 135 (2000).
19. Y. J. Liu, Y. X. Wang, and R. O. Claus, Chem. Phys. Lett. 298, 315 (1998).
20. A. Chandran, "Self-Assembled Multilayered Dielectric Spectral Filters", M.S. thesis, Electrical Engineering Dept., Virginia Polytechnic Institute & State University, Blacksburg, Virginia, September 2001.
21. K. Cooper, "Electrostatic self-assembly of linear and nonlinear optical thin films", Ph.D. dissertation, Electrical Engineering Department, Virginia Polytechnic Institute and State University, Blacksburg, Virginia, May 1996.
22. Y. J. Liu, A. Rosidian, K. Lenahan, Y. X. Wang, T. Zeng, and R. O. Claus, Smart Mater. Struct. 8, 100 (1999).

23. J. R. Heflin, C. Figura, D. Marciu, Y. J. Liu, and R. O. Claus, *Appl. Phys. Lett.* 74 (4), 495 (1999).
24. Y. J. Liu, Y. X. Wang, and R. O. Claus, *Chem. Phys. Lett.* 298 (4-6), 315 (1998).
25. K. Cooper, "Electrostatic self-assembly of linear and nonlinear optical thin films", Ph.D. dissertation, Electrical Engineering Department, Virginia Polytechnic Institute and State University, Blacksburg, Virginia, May 1996.
26. W. H. G. Horsthuis and G. J. M. Krijnen, *Appl. Phys. Lett.* 55, 616 (1989).
27. R. Meyrueix and G. Mignani, *Mater. Res. Soc. Symp. Proc. Ser. 173*, paper Q13.5 (1989).
28. J. F. Valley, J. W. Wu, and C. L. Valencia, *Appl. Phys. Lett.* 57, 1084 (1990).
29. S. Herminghaus, B. A. Smith, and J. D. Swalen, *J. Opt. Soc. Am. B* 8, 2311 (1991).
30. C. C. Teng and H. T. Man, *Appl. Phys. Lett.* 56, 1734 (1990).
31. R. N. Demartino, D. E. Allen, R. Keosian, G. Khanarian, and D. R. Haas, *Mater. Res. Soc. Symp. Proc.* 228, 39 (1992).
32. R. A. Norwood, T. K. Findakly, H. A. Goldberg, G. Khanarian, J. B. Stamatoff, and H. N. Yoon, *Polymers for Lightwave and Integrated Optics: Technology and Applications*, edited by L. A. Hornak (Dekker, New York, 1992), Chap. 11.
33. M. Sigelle and R. Hierle, *J. Appl. Phys.* 52, 4199 (1981).
34. K. D. Singer, M. G. Kuzyk, W. R. Holland, J. E. Sohn, S. J. Lalama, R. B. Comizzoli, H. E. Katz, and M. L. Schilling, *Appl. Phys. Lett.* 53, 1800 (1988).
35. R. A. Norwood, M. G. Kuzyk, and R. A. Keosian, *J. Appl. Phys.* 75 (4), 1869 (1994).
36. B. Swedek, N. Cheng, Y. Cui, J. Zieba, J. Winiarz, and P. Prasad, *J. Appl. Phys.* 82 (12), 5923 (1997).
37. C. Zhang, A. S. Ren, F. Wang, L. R. Dalton, S. S. Lee, S. M. Garner, and W. H. Steier, *Polym. Prepr. (Am. Chem. Soc. Div. Polym. Chem.)* 40, 49 (1999).
38. Y. Shi, C. Zhang, H. Zhang, J. H. Bechtel, L. R. Dalton, B. H. Robinson, and W. H. Steier, *Science* 288, 119 (2000).
39. Y. Shi, W. Lin, D. J. Olson, J. H. Bechtel, H. Zhang, W. H. Steier, C. Zhang, and L. R. Dalton, *Appl. Phys. Lett.* 77 (1), 1 (2000).
40. C. Zhang, M. C. Oh, H. Zhang, W. H. Steier, and L. R. Dalton, *Chem. Mater.* 13, 3043 (2001).
41. J. W. Wu, *J. Opt. Soc. B* 8, 142 (1991).
42. B. Kippelen, K. Sandalphon, K. Meerholz, and N. Peyghambarian, *Appl. Phys. Lett.* 68 (13), 1748 (1996).
43. B. Kippelen, K. Sandalphon, K. Meerholz, and N. Peyghambarian, *Appl. Opt.* 35 (14), 2346 (1996).
44. C. Zhang, M. C. Oh, H. Zhang, W. H. Steier, and L. R. Dalton, *Chem. Mater.* 13, 3043 (2001).
45. D. A. Kleinman, *Phys. Rev.* 126 (6), 1977 (1962).

## VITA

Roger G. Duncan, the son of Wilbur Glenn and Wanda Sue Duncan, was born on September 4<sup>th</sup>, 1978, in Oak Hill, West Virginia. He graduated from Oak Hill high school in May of 1996. In May of 2000 he graduated cum laude from West Virginia University Institute of Technology with a Bachelor of Science degree in Electrical Engineering. Currently, Roger is employed as a research and development engineer by Luna Innovations, Inc., located in Blacksburg, Virginia where he is responsible for research and development in fiber optic sensing technologies and photonic devices. His particular interest currently lay in the field of distributed fiber optic sensing and photonic bandgap materials. This thesis, written in 2002, completes his Master of Science degree in Electrical Engineering from Virginia Polytechnic Institute and State University.